ELSEVIER

Journal of Contaminant Hydrology 58 (2002) 13–49

JOURNAL OF
Contaminant
Hydrology

www.elsevier.com/locate/jconhyd

Bench-scale visualization of DNAPL remediation processes in analog heterogeneous aquifers: surfactant floods and in situ oxidation using permanganate

Stephen H. Conrad *, Robert J. Glass, William J. Peplinski

Flow Visualization and Processes Laboratory, Geohydrology Department, Sandia National Laboratories, P.O. Box 5800, MS 0735, Albuquerque, NM 87185, USA

Received 8 June 2001; received in revised form 28 February 2002; accepted 15 March 2002

Abstract

We have conducted well-controlled DNAPL remediation experiments within a 2-D, glass-walled, sand-filled chamber using surfactants (Aerosol MA and Tween 80) to increase solubility and an oxidant (permanganate) to chemically degrade the DNAPL. Initial conditions for each remediation experiment were created by injecting DNAPL as a point source at the top of the chamber and allowing the DNAPL to migrate downward through a water-filled, heterogeneous, sand-pack designed to be evocative of a fluvial depositional environment. This migration process resulted in the DNAPL residing as a series of descending pools. Lateral advection across the chamber was used to introduce the remedial fluids. Photographs and digital image analysis illustrate interactions between the introduced fluids and the DNAPL. In the surfactant experiments, we found that DNAPL configured in a series of pools was easily mobilized. Extreme reductions in DNAPL/water interfacial tension occurred when using the Aerosol MA surfactant, resulting in mobilization into low permeability regions and thus confounding the remediation process. More modest reductions in interfacial tension occurred when using the Tween 80 surfactant resulting in modest mobilization. In this experiment, capillary forces remained sufficient to exclude DNAPL migration into low permeability regions allowing the excellent solubilizing properties of the surfactant to recover almost 90% of the DNAPL within 8.6 pore volumes. Injection of a potassium permanganate solution resulted in precipitation of MnO_2, a reaction product, creating a low-permeability rind surrounding the DNAPL pools. Formation of this rind hindered contact between the permanganate and the DNAPL, limiting the effectiveness of the remediation. From these experiments, we see the value of performing visualization experiments to

* Corresponding author. Tel.: +1-505-844-5267; fax: +1-505-844-6023.
E-mail address: shconra@sandia.gov (S.H. Conrad).

0169-7722/02/$ - see front matter
PII: S0169-7722(02)00024-4

evaluate the performance of proposed techniques for DNAPL remediation.

Keywords: Remediation; Surfactants; Potassium permanganate; DNAPL; Trichloroethylene; Porous media; Laboratory measurement

1. Introduction

Over the past decade, surfactant-enhanced remediation has been studied as a promising remedial technique for cleaning up spilled organic solvents. More recently, oxidation techniques have been proposed. The path for demonstrating the efficacy of any remediation technique typically begins with proof-of-concept studies carried out as batch experiments and as displacements in laboratory columns. Column studies provide an essential first step, and while good experimental control can be maintained, they lack representativeness to field situations. In contrast, pilot-scale field studies can provide representativeness, but some experimental control is inevitably sacrificed. Both of these types of experiments operate largely as ''black boxes'' in that it is difficult to directly monitor the interactions between the contaminant, the treatment fluid, and the aquifer material. Interpretation of results is typically dominated by analysis of the effluent. Two-dimensional ''sandbox'' experiments can be conducted to allow for visual observation of the remediation process. Sandbox experiments can bridge the gap between column studies and field-scale pilot studies in that they can be constructed to be somewhat more representative of field conditions while maintaining good experimental control. In this paper, we describe sandbox experiments we have conducted to study surfactant-enhanced remediation and in situ oxidation for remediation of separate-phase TCE. The remainder of this introduction is devoted to briefly reviewing previous work in DNAPL remediation using surfactants (Section 1.1) and permanganate as an oxidant (Section 1.2).

1.1. Surfactant studies

A large number of studies have been undertaken to investigate using surfactants to remediate NAPLs. At concentrations exceeding the critical micelle concentration (CMC), surfactant molecules aggregate to form micelles that greatly enhance the solubility of organic-phase constituents in water. Above the CMC, solubility increases as a linear function of surfactant concentration. By boosting solubilities by several orders of magnitude, the efficiency of pump-and-treat can be increased to the point that it becomes a viable remedial option. At the same time, surfactants also lower water/organic interfacial tensions, thereby reducing capillary forces. If capillary forces become sufficiently small relative to viscous and gravity forces, mobilization of the NAPL may result. Indeed, inducing this mobilization is the intent in enhanced oil recovery. Mobilization may also significantly improve recovery efficiency in the case of spilled LNAPLs (e.g., Knox et al., 1999). However, mobilization of DNAPLs is to be avoided because it may lead to uncontrolled downward migration that can undermine remediation rather than enhance it.

Trade-offs must be made between enhancing solubility and reducing the potential for downward DNAPL mobilization. The Chun-Huh relationship (Pope and Wade, 1995) postulates that the interfacial tension is inversely proportional to the square of the solubilization potential. Therefore, we must accept less solubility enhancement and less efficiency if we want to keep the interfacial tensions high to reduce the potential for inadvertent mobilization. Conversely, if we are willing to accept low interfacial tensions, then very efficient displacement of the organic phase can be achieved through the formation of stable, middle-phase microemulsions. These are created at high surfactant concentrations and with additional variations (such as salinity adjustment or addition of a cosolvent) to promote location of the surfactant at the organic/water interface. Shiau et al. (1994) showed that middle-phase microemulsions could accommodate organic concentrations of at least one or two orders of magnitude greater than surfactant systems geared toward solubilization. However, middle-phase microemulsion systems produce ultra-low interfacial tensions, on the order of 10^{-3} to 10^{-4} dyn/cm.

There are several schools of thought about how to handle the trade-off between increasing solubility and lowering interfacial tensions. Some researchers advocate taking a conservative approach and encourage the use of surfactants that minimize interfacial tension reductions (e.g., Fountain et al., 1991, 1995, 1996; Pennell et al., 1994, 1996; Taylor et al., 2001) while others (e.g., Baran et al., 1994; Pope and Wade, 1995; Martel et al., 1998a,b; Dwarakanath and Pope, 2000) suggest that more efficient recovery can be achieved by using surfactant formulations that either (1) increase the solubilization potential, (2) mobilize DNAPL via formation of an oil bank, or (3) mobilize DNAPL via formation of a middle-phase microemulsion. These more aggressive options may be viable in cases where site specific factors may mitigate the potential for downward mobilization such as having a small organic/aqueous density difference or having a fine-textured underlying confining layer of sufficient integrity to prevent DNAPL penetration once interfacial tensions are lowered. Recently, Sabatini et al. (2000) proposed a hybrid approach where interfacial tensions are maintained above those required to induce mobilization for the first several pore volumes of the surfactant flood. The assumption here is that the most mobile DNAPL is solubilized during this time. Over time, the surfactant formulation is modified to create more efficient solubilization (and correspondingly lower interfacial tensions). Finally, a middle-phase microemulsion system would be employed.

Numerous batch experiments have been conducted to assess the ability of various surfactant formulations to solubilize a variety of commonly spilled solvents (e.g., Fountain et al., 1991; Shiau et al., 1994; Okuda et al., 1996; Pennell et al., 1997). Baran et al. (1994) produced classical Windsor-type phase behavior for TCE and CCl_4 using anionic surfactants and varying the salinity. Martel et al. (1993) used phase diagrams of surfactant/water/organic systems to create microemulsions using high surfactant/cosolvent concentrations. They showed that the lower the miscibility curves in phase diagrams, the more efficient the recovery process. Mayer et al. (1999) used batch studies to assess the potential for chemical reaction rate limitations to affect mass-transfer rates. Dwarakanath et al. (1999) identified rapid formation of microemulsions as a requirement for surfactant selection. Dwarakanath and Pope (2000) found that using pure-component DNAPLs in batch studies can be useful for selecting suitable surfactants for complex multicomponent field DNAPLs. St.-Pierre et al. (2000) used phase diagrams to predict the dominant

displacement mechanism—solubilization versus mobilization—for various surfactant formulations.

A number of column studies have examined the conditions required for the onset of mobilization. Pennell et al. (1994) showed that ultra-low interfacial tensions are not required to induce mobilization. Longino and Kueper (1995) showed in a vertical 1-D column that sufficient upward hydraulic gradient could be used to counteract reduction of interfacial tension during surfactant flushing to prevent downward mobilization of a DNAPL pool. Pennell et al. (1996) used column experiments to investigate the onset and extent of mobilization during surfactant flushing. They developed the trapping number concept (discussed in more detail in later) that relates viscous and buoyancy forces to the capillary forces, which act to hold trapped organic liquids in place. Other researchers have since used the trapping number concept successfully to predict the occurrence of mobilization of trapped residual NAPL saturations in laboratory columns (e.g., Dwarakanath et al., 1999; Boving and Brusseau, 2000).

A number of column studies have examined rate limitations during micellar solubilization. Pennell et al. (1994) saw rate limitations in recovery based on (1) a disparity between concentrations of PCE in column effluent and equilibrium concentrations and (2) increased effluent concentrations following flow interruptions. Several researchers have used column studies to apply mass transfer models for solubilization (e.g., Abriola et al., 1993; Fortin et al., 1997; Mayer et al., 1999; Schaerlaekens et al., 2000). While all these models successfully predicted effluent concentrations, Fortin et al. (1997) found that upon destructive sampling at the conclusion of the experiments, the model they used did a poor job of describing NAPL distributions remaining in the columns. They suggested that effluent concentrations alone might be insufficient to infer the nature of displacement processes occurring in laboratory columns. Recently, Zhong et al. (2001) conducted 2-D glass micromodel studies and observed that microscale dissolution fingering may contribute to nonequilibrium mass transfer rates in surfactant/NAPL systems, similar to that seen previously for pure water/NAPL systems (Imhoff et al., 1996). Interestingly, Dwarakanath et al. (1999) reported improved solubilization efficiencies when using xanthan gum polymer for mobility control in lab columns. We conjecture that the polymer may improve efficiency in part by suppressing the formation of dissolution fingers.

Several pilot-scale field studies have been conducted. Excellent DNAPL recoveries (in excess of 95%) have been reported in field tests conducted in relatively homogeneous aquifers (Brown et al., 1999; Hasegawa et al., 2000). Less complete recoveries have been reported in field tests where heterogeneities caused DNAPL to be retained in layers that had not been effectively swept by the surfactants (Fountain et al., 1995, 1996; Holzmer et al., 2000).

Several heterogeneous 2-D sandbox studies have been conducted within the last few years. Typically, these involve fine-textured lenses imbedded in a coarse matrix. DNAPL migrates downward from the top and becomes pooled on the fine-textured lenses. Some of these studies have reported downward mobilization and/or penetration into fine-textured layers once surfactant encountered the pooled DNAPL (Walker et al., 1998; Oostrom et al., 1999; Ramsberg and Pennell, 2000). Others have investigated the additional mass transfer limitations imposed by heterogeneities—that is, the low interfacial areas for pooled DNAPL, and the bypassing of aqueous-phase flow around the pools (Rathfelder et al., 1998; Taylor et al., 2001).

1.2. Permanganate studies

A number of permanganate studies have been conducted in recent years. Batch experiments have been used to determine reaction kinetics for permanganate oxidization of chlorinated solvents (Yan and Schwartz, 1999; Urynowicz and Siegrist, 2000). Results from column studies with a residual DNAPL source show nearly complete degradation of chlorinated solvents (Schnarr et al., 1998; Li and Schwartz, 2000). However, Li and Schwartz (2000) did report column plugging by precipitating MnO_2, a reaction product of the oxidation. In this experiment, reaction rates decreased markedly with time as the MnO_2 precipitate caused mass transfer limitations.

Several pilot-scale, permanganate field studies have been performed. For a relatively fledgling remedial technology, it is interesting to note the predominance of field studies. In instances where the DNAPL source was well mixed with soil to resemble a source zone at residual saturation, nearly complete removal was achieved (Schnarr et al., 1998; Thompson et al., 2000). However, in an experiment where DNAPL was allowed to infiltrate into the aquifer, creating a more representative initial condition, more than one-third of the DNAPL remained in the aquifer after 290 days of flushing (Schnarr et al., 1998). In other permanganate studies in which pooled DNAPL was present, cores extracted at the conclusion of the experiment revealed incomplete oxidation of the DNAPL and MnO_2 precipitation in the vicinity of the DNAPL pools (Huang et al., 2000; Nelson et al., 2000). Here again, it has been hypothesized that the efficiency of mass transfer of the reactants in the aqueous phase may decrease as MnO_2 precipitates at the mass transfer paths. However, Mott-Smith et al. (2000) reported a lack of significant formation plugging at their permanganate field test site at Cape Canaveral.

Several 2-D sandbox studies have been conducted as well. Li and Schwartz (2000) conducted a permanganate flush using a small homogeneous flow cell. One milliliter of TCE was allowed to infiltrate to create the initial condition of TCE configured as a residual finger leading to TCE pooled on the bottom of the cell. The TCE finger oxidized rapidly, but reaction rates were much lower for the pooled TCE. A low-permeability rind of precipitated MnO_2 rapidly formed above the TCE pool causing flow to bypass the pool. Likewise, Thompson et al. (2000) performed a permanganate flush on pooled DNAPL and used chloride, another reaction product, to track the progress of the oxidation. A decrease in effluent chloride concentration over time indicated a decreased oxidation rate that is believed to be related to formation of MnO_2 deposits at the pool interface. Excavation at the conclusion of the experiment revealed precipitated MnO_2 in the vicinity of the DNAPL source region. Reitsma and Marshall (2000) pooled DNAPL in a coarse lens in an otherwise homogeneous sand pack. During permanganate flushing, production of both MnO_2 and CO_2 was observed and it was hypothesized that production of both these reaction products caused a significant change in the flow patterns.

2. Experimental design

We designed experiments within a thin but extensive sand chamber where we could use quantitative light transmission visualization techniques (e.g., Tidwell and Glass, 1994) to

record remediation dynamics in time. Using a computer-automated sand packing procedure, a reproducible heterogeneous structure was constructed to be reminiscent of fluvial lithologies. Initial conditions were established by injecting TCE under constant flux, gravity destabilized conditions. Horizontal flow between manifolds stretching the length of the chamber's vertical sides allowed for the introduction of fluids simulating inter-well remediation floods. This experimental design provided a realistic analog to field-scale remediation processes allowing us to visually observe the interaction between DNAPLs, the remedial fluids, and the heterogeneous aquifer material. With this design, direct comparison of the remedial techniques to one another was also possible.

2.1. Chamber construction

The chamber was constructed of two plates of glass (1.90 cm thick) held apart by two steel side rails (1 cm thick) that ran down the vertical edges of the glass. The internal dimensions of the chamber were 1-cm thick (~10–40 pores/grains) by 60.5-cm wide by 60-cm tall. Viton o-rings embedded in the side rails provided a seal with forces applied by an external clamp running the length of the chamber sides. Screen covered manifolds, running the length of the side rails, were connected to inflow and outflow tubing. An additional port within each side manifold was connected to a manometer. At the top and bottom, a screened manifold and a porous plate, respectively, were sealed to the chamber allowing for vertical filling and drainage of water. Steel bars were clamped horizontally to the outside of the glass plates at the top and bottom to minimize bowing of the glass chamber walls under the pressures created by filling the chamber with sand and fluids. Such bowing allows sand grains to redistribute, adversely affecting the image analyses and slightly changing the pore structure and the volume inside the chamber.

2.2. Chamber packing

Four translucent, hydrophilic silica sands with slightly overlapping grain size distributions comprised the units within the heterogeneous sand pack. These sands range in texture from coarse to fine sand and their properties are given in Table 1. These sands provided permeabilities that ranged over a factor of ~20, and a capillary contrast for nonwetting fluid entry that ranged over a factor of ~4. Pressure-saturation curves for three of these sands measured within the chamber geometry were reported in Glass et al. (2000). Properties of comparable sands within standard column configurations have been measured and reported by Schroth et al. (1996).

Table 1
Sand properties

Sand	Sieve size	Grain size [minimum, mean, and maximum (mm)]	Porosity	Intrinsic permeability (cm^2)
Course	12–20	0.84, 1.1, 1.7	34.8	6.32×10^{-6}
Medium-course	20–30	0.50, 0.71, 1.0	34.8	2.55×10^{-6}
Medium	30–40	0.42, 0.53, 0.60	35.4	1.20×10^{-6}
Fine	50–70	0.21, 0.26, 0.30	36.2	2.97×10^{-7}

The chamber was filled using a procedure designed to create reproducible facies-like geometric structures (Glass et al., 2000). After filling the chamber, we settled the sand using capillary forces. The capillary forces were provided by filling the chamber with de-aired, deionized water followed by water drainage. This procedure was repeated several times until settling was complete. Details are provided elsewhere (Glass et al., 2000). At the top of the chamber, modeling clay was packed in between the ports of the top manifold to ensure a tight seal between the manifold and the sand. The pore volume of the chamber was approximately 1475 ml for each of the experiments. This volume varied a small amount between packings due to minor variations in the assembly of the chamber from one experimental trial to the next.

The heterogeneity structure used in these experiments is shown in Fig. 1. This structure was designed to qualitatively represent fluvial depositional environments where textures vary sharply across facies boundaries. It was also designed so that migrating DNAPL would avoid hitting any of the four lateral boundaries of the chamber (top, bottom, and sides). As will be discussed in more detail later, we were not entirely successful in this regard. We used two different sand packs for our experiments. The first sand pack is shown in Fig. 1. In the second sand pack, pool #7 was made somewhat deeper so that it would be more likely to capture TCE that continued to migrate during redistribution, once the injection of TCE into the chamber had ceased.

2.3. Image acquisition and processing

The experimental chamber was placed in front of a controlled output, diffuse light source. All phases of the experiments were documented with both color 35 mm photographs and digital images of the transmitted light field. Digital images were captured using a 1024×1024 pixel, 4096 gray level, shuttered, monochromatic, Charge Coupled Device (CCD) camera. Digital images had a resolution of ~0.6 mm per pixel (0.36 mm^2/pixel) and were intensity adjusted for small temporal changes in the light source and aligned for small subpixel shifts over the full course of an experiment. Details of the digital method and processing can be found elsewhere (Glass et al., 2000). (Offsets in camera position account for slight differences in perspective between the digital images and the 35 mm photographs.)

During remediation experiments, several factors influenced the light transmission through the pack. Oil-Red-O dye was added to the TCE to enhance visibility. Therefore, changes in TCE saturation affected light transmission. If that had been the only influence, we could have used changes in light intensity to quantitatively track the removal of TCE from the chamber during each remediation experiment. However, several confounding factors made that approach untenable. First, introduction of the remedial fluids affected light transmission. For example, the presence of salt in one of the surfactant solutions caused an increase of light transmission behind the flood front, while conversely, introduction of purple potassium permanganate decreased light transmission. Also, in the permanganate in situ oxidation experiment, creation of opaque reaction products decreased light transmission. While these effects were beneficial because they allowed us to actually see the progression of the flood fronts and the reaction processes, they adversely affected our ability to quantify TCE removal. Likewise during the surfactant experiments, TCE dye concentration changes occurred during the solubilization process because the TCE was

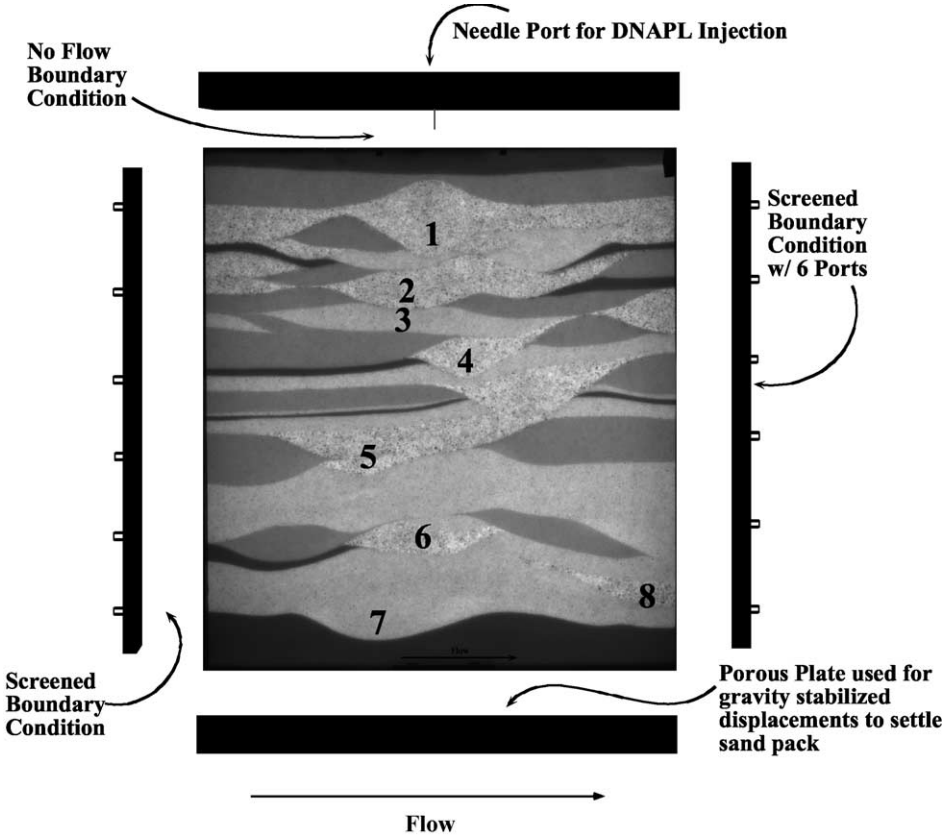

Fig. 1. A digital image of a heterogeneous sand pack used in the remediation experiments. In this image, the coarse sand transmits the most light and hence is the lightest; the medium-coarse sand appears light gray in color; the medium sand appears as a darker gray; the fine sand appears dark. TCE was injected from the needle port located at the top-center of the sand pack. Aqueous phase flow occurred from left to right through the screened manifolds on either side of the chamber. The top and bottom served as no-flow boundaries for aqueous flow. The numbers indicate the locations of pools that form during the downward migration of TCE. These pools are identified by number in the text.

more readily solubilized than the dye. Finally, we note that the rather large disparity in light transmission over the range of sand textures caused us some exposure problems in the fine sand and at the abrupt transitions in texture at facies boundaries, thus affecting our ability to digitally image changes in saturation. It is because of this array of confounding factors that we have used the digital images primarily to display qualitative spatial and temporal differences that occur during the course of the experiments.

2.4. Overview and sequencing of experimental activities

A brief discussion of the sequence of experiments will be helpful to understand the small variations in initial conditions between each of the three remediation experiments.

In the first sand pack, we conducted a remediation experiment using MA, an anionic surfactant. We began by injecting TCE into an initially water-saturated sand-filled chamber to establish the initial conditions for the remediation experiment. We terminated injection just as the TCE finger touched the bottom aquitard (67 ml TCE). A significant amount of redistribution occurred once injection ceased, allowing TCE to reach the side of the chamber and enter the downstream manifold. Once redistribution had ceased, the Aerosol MA experiment was conducted. Entry of TCE into the side manifold may have confounded our interpretation of dissolved TCE measured in effluent from the chamber. At the conclusion of this experiment, we cleaned and refilled the chamber with sand, making pool #7 larger.

In this second sand pack, we conducted a series of tests, consisting of: (1) side-to-side injection of a blue dye pulse in the aqueous phase to examine aqueous flow behavior through the sand-filled chamber, (2) a second surfactant experiment using Tween 80, a nonionic surfactant, (3) a partitioning inter-well tracer (PIT) characterization test (not reported on here), and (4) a third remediation experiment using potassium permanganate as an in situ oxidant.

This sequence of experiments began by pushing a side-to-side aqueous-phase blue dye pulse through the chamber. Following the blue pulse, the TCE was injected to establish initial conditions for the Tween 80 surfactant experiment. Injection of TCE was terminated when the capillary barrier beneath pool #6 was just breached (54 ml TCE). However, upon redistribution, TCE still entered the side manifold. Subsequent to the TCE injection, another blue pulse was pushed through the chamber. By comparing the preinjection and postinjection pulses, we were able to see the effect of the TCE on the aqueous flow field. The postinjection pulse resulted in some dissolution of TCE prior to the beginning to the Tween 80 experiment.

The Tween 80 remediation experiment was then conducted. At the conclusion of the experiment, additional Tween 80 surfactant was injected from the bottom manifold in order to solubilize the remainder of TCE present in pool #7. Removal of the TCE was followed by injection of 76 pore volumes of water to assure complete removal of the surfactant solution, thus allowing us the opportunity to reuse this sand pack.

Prior to TCE injection for the permanganate experiment, we used image analyses from the first two experiments to calculate an injection volume that would not reach the side manifold. For this injection, we stopped injecting after 37 ml TCE, as pool #6 was still filling. This time, no TCE entered the side manifold. With TCE finally in a completely proper configuration in the sand pack, we decided to conduct a PIT test prior to conducting the permanganate flood. However, when we conducted the PIT test on this configuration, additional TCE redistribution occurred and once again TCE entered the side manifold. This additional redistribution presumably occurred due to hydraulic stresses imposed by beginning the PIT flood. Redistribution began concurrent with the start of the PIT flood, long before the tracers could have encountered the TCE. Chemical interaction between the alcohol tracers used in the PIT test markedly increased the solubility of TCE. Digital analysis comparing images taken prior and subsequent to the PIT test confirms that some dissolution of the TCE had occurred. Once the PIT test was completed, we conducted the permanganate experiment.

The TCE injections allowed us to recreate realistic and nearly identical TCE distributions within the main part of the chamber for each remediation flood. However, the

presence of TCE in the downstream manifold creates some uncertainty about the validity of the effluent concentrations we measured and thus they are not reported in this paper.

3. TCE migration and influence on the aqueous flow field

Each TCE injection started with the aquifer filled with de-aired, deionized water. A fully water saturated state was verified with the light transmission method. An 18-gauge needle (0.84 mm ID) was inserted in the middle of the top manifold downward through the top fine layer and into the underlying coarse layer. TCE was injected through the needle via a syringe pump at a rate of 0.25 ml/min for all experiments. This rate was determined as the lowest repeatable rate attainable with the available pump. (TCE tended to bind up the grease on the syringe and at lower rates the injection was unsteady.) During injection, the outflow of water from the side manifolds was measured gravimetrically every 30 s to verify that a constant injection rate was being maintained. In Figs. 2 and 3, we illustrate TCE migration and its influence on the flow of water through the chamber using the first TCE injection into the second sand pack. (This is the injection that established initial conditions for the Tween 80 surfactant experiment.)

As we discussed in detail elsewhere (Glass et al., 2000, 2001) DNAPL migrates under the combined influence of gravity, capillary, and viscous forces. Heterogeneities in media texture result in TCE occupying a series of pools separated by fingers as exemplified in Fig. 2A. As invasion progresses, a gravity-driven finger moves down until it encounters a capillary barrier formed by a finer textured unit. Continued invasion then proceeds by filling the region above the capillary barrier forming a pool of high saturation, approaching the nonwetting phase satiated saturation value of ~ 0.83 (the maximum nonwetting phase saturation measured from the pressure saturation curves). The pool continues to fill until it reaches a maximum height where sufficient pressure has been achieved to overcome the capillary pressure resisting displacement through the capillary barrier. At this time, the capillary barrier is breached by fingers, which then continue to grow downward beyond the capillary barrier. These fingers continue migrating down to the next barrier where the process is again repeated. We show a composite invasion image in Fig. 2B that summarizes the invasion process using color to represent the temporal sequence of the advance of the TCE invasion front.

Once injection was terminated, TCE continued to migrate. Because our flow rate was high enough that viscous forces were nonnegligible, we had substantial redistribution after injection was terminated. Fig. 2C shows a difference image between the final injection image and the final state as shown in Fig. 2A. Light regions show where TCE has migrated to; dark regions show where it migrated from. As can be seen, a significant amount of redistribution has occurred after the capillary barrier beneath pool #6 was breached. A large pool (#7) formed that covered most of the bottom aquitard. Additionally, TCE entered the downstream manifold through the screen, rose within the manifold, and reentered the chamber through a coarse unit adjacent to the manifold to form a pool there (indicated as pool #8 in Fig. 1).

During all three TCE migration experiments, we found that as invasion proceeded, pulsation occurred within both fingers and pools (see Fig. 2D). The maximum height of

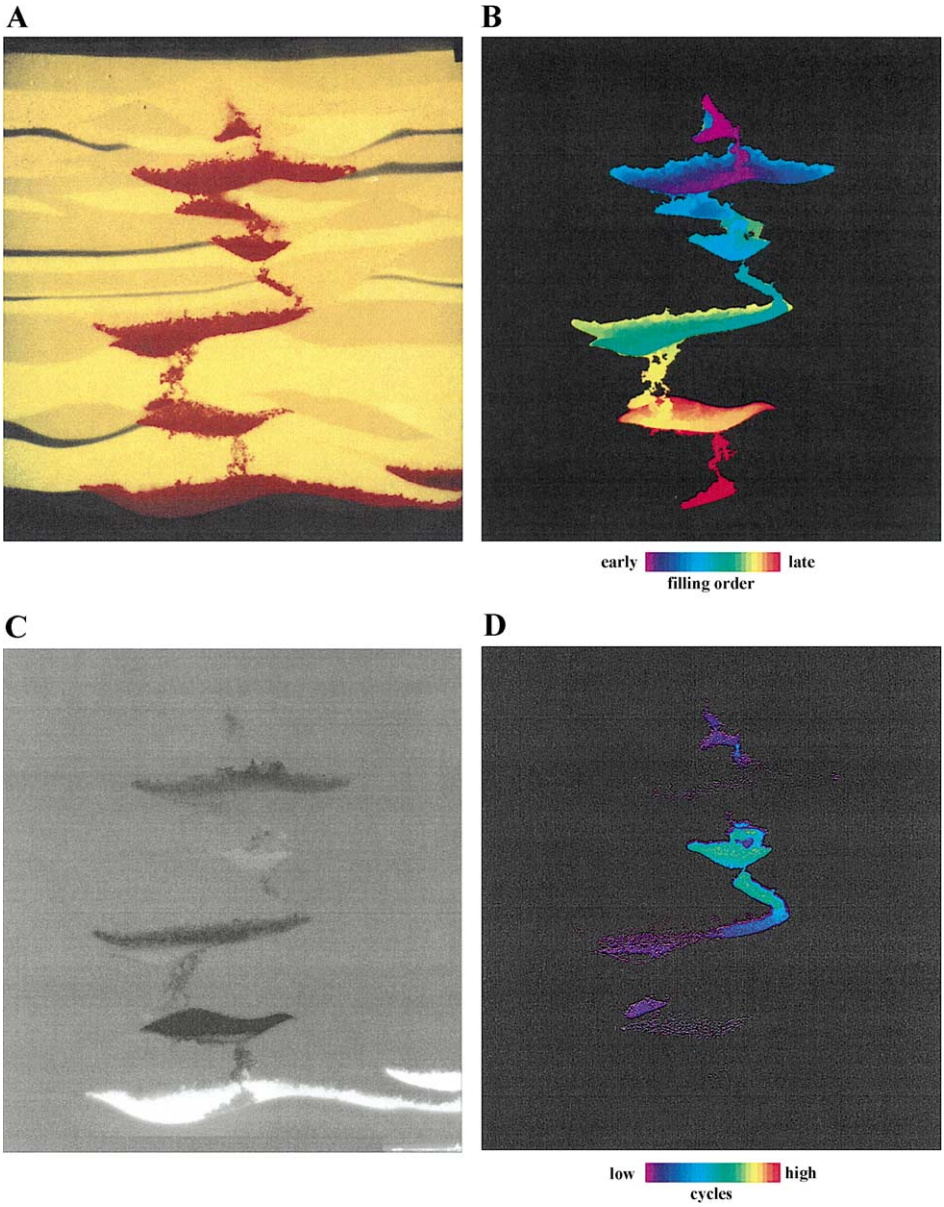

Fig. 2. A summary of TCE migration through the heterogeneous sand pack: (A) a photograph of red-dyed TCE configured into a series of pools interconnected by fingers; (B) a composite image showing the sequence of TCE invasion—the color represents the order in which TCE displaced water; (C) a difference image showing the redistribution of TCE once injection was stopped—dark zones indicate locations from where TCE has drained and light regions indicate locations to where the redistributed TCE has migrated (gray indicates no change); (D) an image showing pulsation of TCE saturation during the injection of TCE—the color represents the number of cycles of saturation increase then decrease.

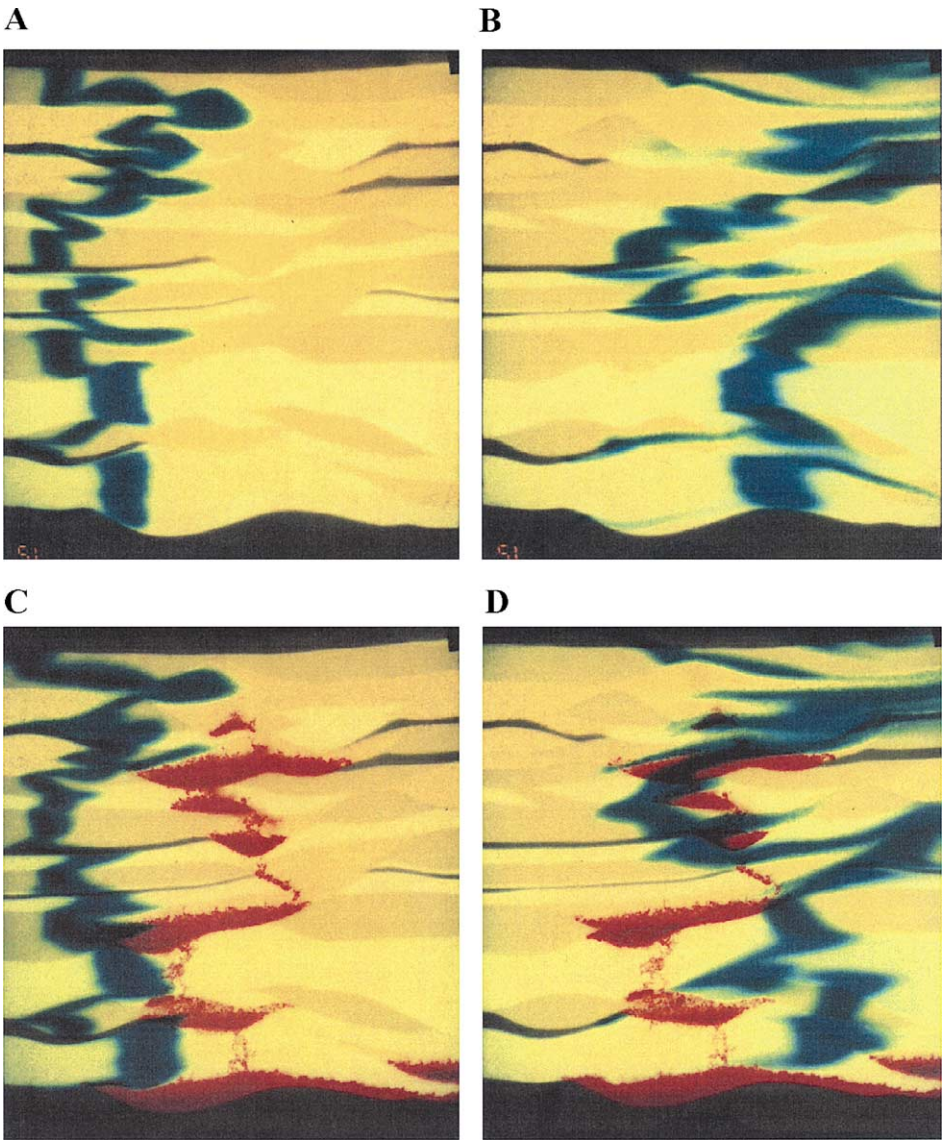

Fig. 3. Photographs showing the character of aqueous-phase flow. A pulse of blue dye tracks the progress as water flows laterally across the chamber from left to right prior to the injection of TCE: (A) 0.14 pore volumes; (B) 0.51 pore volumes. Another pulse was introduced subsequent to the injection of the TCE: (C) 0.14 pore volumes; (D) 0.51 pore volumes.

the pool is determined by the balance of gravity, capillary, and viscous forces. Once the barrier is breached, the interaction of hysteretic capillary forces and gravity can cause the pool to drain. The pool will continue to drain until the pressure drops sufficiently for critical pores within the barrier to become reinvaded with water. Once this occurs, the pool height

must once again increase to the maximum value to breach the barrier. Pulsation occurs most readily when viscous forces are low. As flow rate increases, the increase in viscous forces has been found to damp the pulsation process. Previously, we have described this process and developed functional relations for pool heights and pulsation (Glass et al., 2000). The scale analysis presented there predicts the onset of pool throbbing shown in Fig. 2D. Notice from the figure that pool #4 fills and drains multiple times during the TCE invasion.

Given the injection volumes for the three TCE injections, effective TCE saturations in these experiments (considered over the entire chamber volume) ranged from ~2.5% to ~4.5%. These saturations are much lower than the residual saturations typically measured in 1-D laboratory columns (anywhere from 15% to 40%). In contrast to the stable invasion and displacement process commonly performed to arrive at the initial conditions for a column experiment, unstable invasion combined with the presence of heterogeneities controls the migration process and configures the majority of the TCE mass into a series of high saturation pools. Far less of the TCE is configured as residual saturation, occurring above pools that have partially drained (either by pulsation or redistribution) or where a gravity driven finger has formed and subsequently drained. It is important to realize that during TCE injection and redistribution, the vast majority of the aquifer material was never contacted by TCE. So what we have is a small portion of the aquifer material holding TCE at high saturation (as opposed to TCE held as residual saturation distributed widely throughout the aquifer). And because the TCE held in pools is continuous, it constitutes a large and potentially mobile source that is currently held in lithologic capillary traps where coarse textured sediments directly overlie a finer textured unit. Pools have the potential to form in coarse facies throughout an aquifer, not just on the bottom (e.g., Conrad et al., 1989; Wilson et al., 1990; Kueper et al., 1993; Brewster et al., 1995). Additionally, we expect pools to form at a variety of scales within facies due to interfacies heterogeneity.

We measured the effective permeability both before and after TCE injection. At the same time, we followed the movement of a blue dye pulse through the chamber both before and after TCE emplacement to give some indication as to the paths that the fluids would take. Fig. 3 shows the progression of dye through the chamber and its hydraulic interaction with the pools of TCE. Prior to the start of the blue dye pulse, the inlet manifold was flushed with dye solution to eliminate any spurious "wellbore mixing" effects and to provide a dye pulse that was even along the entire length of the manifold. This same procedure was used for introduction of all other aqueous phase floods. Constant flux rates for all aqueous phase floods were achieved using a peristaltic pump and an inline pulse dampener. All floods were conducted at a flux rate of ~5 ml/min. During flooding, the outflow of water from the downstream side manifold was measured gravimetrically every 30 s to verify that a constant flux rate was being maintained.

Differences in permeability between facies affected the uniformity of all aqueous phase floods—dye tracer, surfactants, and permanganate. Differences in dye pulses performed before and after DNAPL emplacement reveal that the presence of DNAPL changed the permeability field somewhat by lowering the permeability to water in the coarse facies where TCE pools had formed. The presence of DNAPL resulted in a decrease in the bulk permeability of the chamber by ~35%. Slow movement of the dye pulse through and around the TCE pools appeared to enhance the bulk-scale dispersion. Animation of the

blue dye pulse revealed that the bottom pool (#7) is largely bypassed by aqueous phase flow. Of course, this has implications for the remediation floods to follow.

Digital analysis comparing images taken prior and subsequent to injection of the second dye pulse (not shown) revealed that some TCE dissolution had occurred. The dissolution occurred predominantly in the residual present as fingers and along the tops of the pools. Were this slow dissolution process to continue for an extended time period—as would be expected to occur in field situations—the residual DNAPL would continue to be preferentially dissolved leaving only the pools.

4. Remediation floods

Three separate remediation experiments were conducted, two using surfactant floods (Aerosol MA and Tween 80) and one using a solution of potassium permanganate. We present the results for each of these experiments in turn.

Remedial fluids were introduced through the left vertical side manifold. Fluids for all three remediation experiments were introduced at a flow rate of ~5 ml/min. At these flow rates, injection of a pore volume of remedial fluids required ~295 min (nearly 5 h). This represents an effective velocity of ~0.2 cm/min. Initial hydraulic gradients across the chamber were on the order of about 0.007 for the remediation experiments providing a reasonable analogue to typical field conditions.

4.1. Aerosol MA surfactant experiment

In our first of two surfactant experiments, the anionic surfactant Aerosol MA (sodium dihexyl sulfosuccinate) was injected. This surfactant has been used previously by several researchers (e.g., Kostarelos et al. 1998; Mayer et al., 1999; Dwarakanath et al. 1999; Brown et al., 1999) and the phase behavior for this surfactant has been studied by Baran et al. (1994). The surfactant composition for this experiment was 1.6% Aerosol MA, 4% isopropanol, and 0.3% NaCl in de-aired, deionized water. The objective for this formulation was to maximize solubilization and minimize mobilization to the extent possible. However, even so, the interfacial tension between TCE and the surfactant was quite low, having been measured to be 0.62 dyn/cm (Zhong et al., 2001).

Fig. 4A is a photo showing the TCE as it was configured in the sand-filled chamber prior to invasion by the Aerosol MA surfactant. (Compare this TCE configuration to the configuration shown in Fig. 2A for the first TCE injection in the second sand pack.) The surfactant solution migrated toward the TCE from left to right in a jagged pattern similar to that created by the injected dye pulse (Fig. 3C). Fig. 4B shows the beginnings of mobilization just after the surfactant front had encountered TCE at 0.29 pore volumes injected. Fig. 4C shows the differences in light intensity between digital images taken at times corresponding to the photos shown in Fig. 4A,B. Dark regions show where the light intensity has increased, indicating locations from where the TCE has migrated. White regions show where the light intensity has decreased, indicating regions to where the TCE has migrated.

As can be seen from Fig. 4B,C, the surfactant front has encountered the left side of three TCE pools (pools #2, #5, and #7) and mobilization of TCE has begun. Close-up

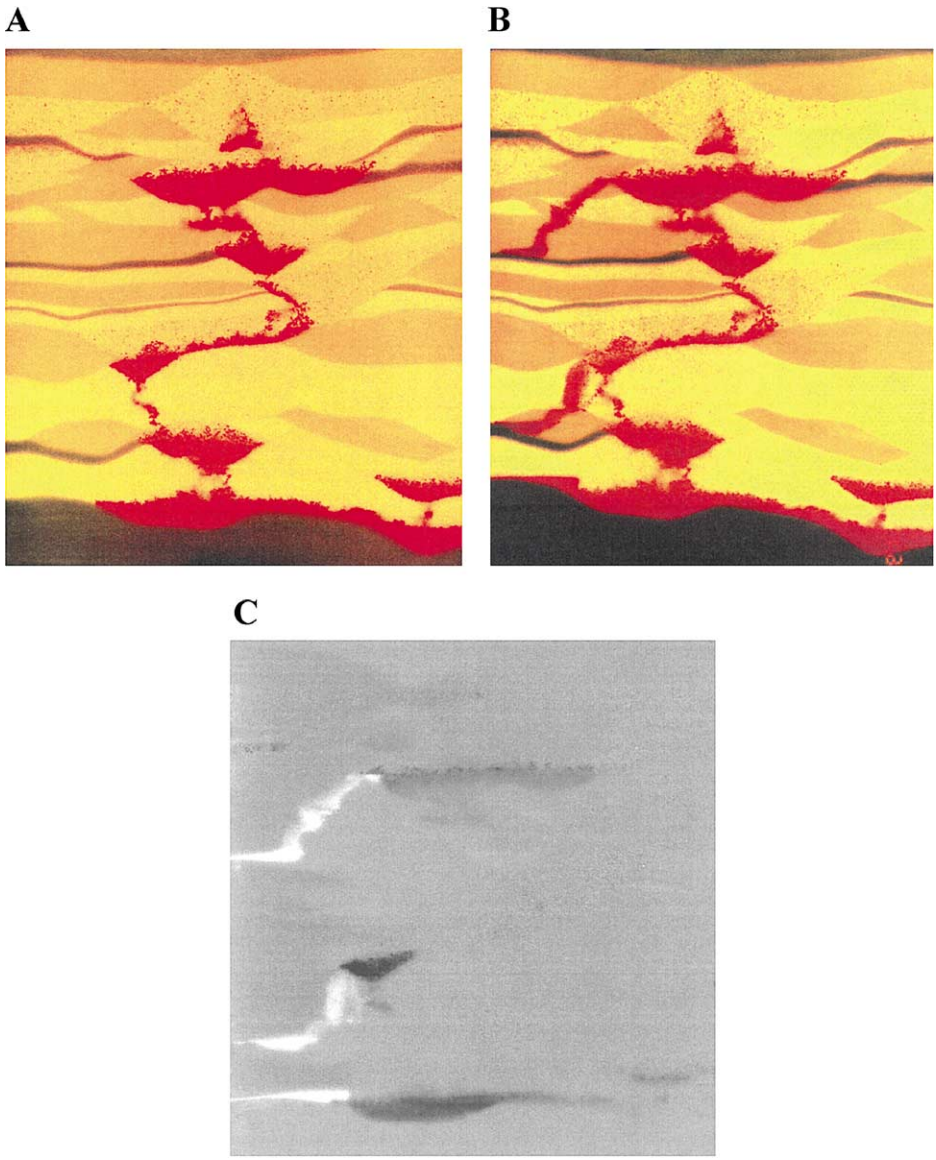

Fig. 4. Images from the start of the Aerosol MA surfactant experiments: (A) a photograph showing the configuration of the TCE prior to the surfactant flood; (B) a photograph showing the beginning of mobilization as the surfactant flood first encountered TCE at 0.29 pore volumes; (C) an image showing differences in light intensity between a digital image taken at 0.29 pore volumes and an image taken prior to the start of the surfactant flood—dark regions show from where TCE has migrated, while white regions indicate regions where TCE has migrated into (gray indicates no change).

photographs of mobilization from pools #2 and #7 in Fig. 5 provide additional detail. In these pools, high interfacial tensions ahead of the front coupled with low interfacial tensions behind the front created a pressure differential inducing mobilization of the TCE and drainage of the pools. Behind the surfactant front, reduction in interfacial tension caused a reduction in the capillary forces that had previously held the TCE in place. We call this mobilization mechanism a "capillary bellows"; the specifics of which are discussed in detail in the section entitled *Predicting the onset of mobilization* below.

In Fig. 5A, notice that in the absence of strong capillarity, the TCE migrating from pool #2 has moved downward under the force of gravity, but also against the prevailing hydraulic gradient (higher aqueous phase pressures are to the left). Similarly, Zhong et al.

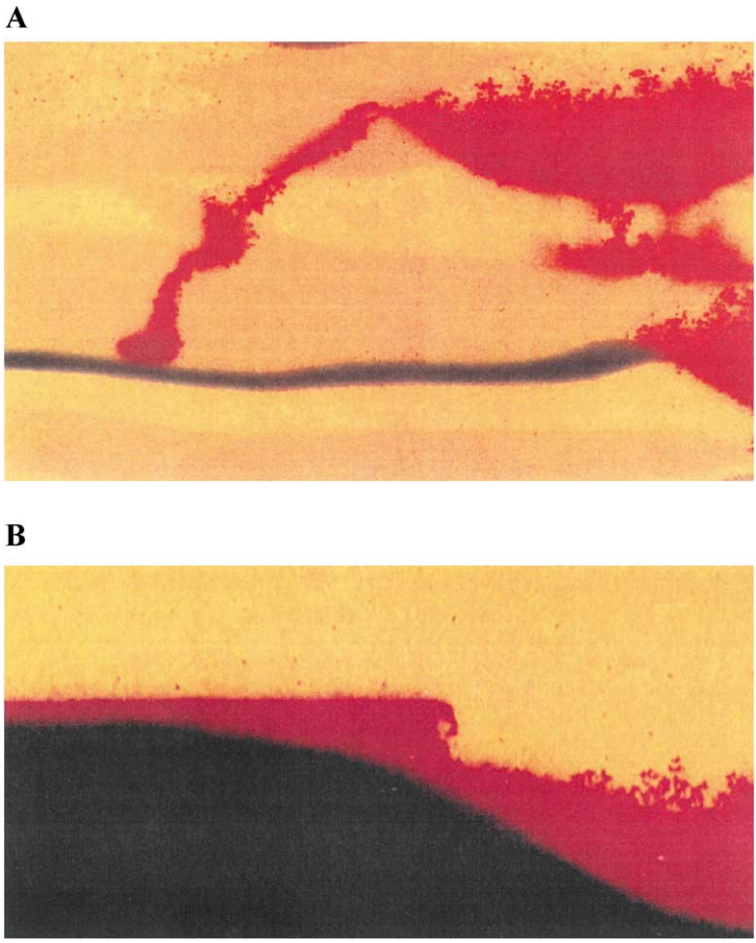

Fig. 5. Close-up photographs of TCE mobilization from the Aerosol MA surfactant flood at 0.29 pore volumes: (A) upstream and downward mobilization from the left side of pool #2; (B) upstream and upward mobilization from the left side of pool #7.

(2001) working on a smaller scale in glass micromodels observed the upstream migration of previously trapped NAPL blobs upon contact with the surfactant flood front thereby contributing to formation of an oil bank. They also attributed this behavior to capillary force imbalances due to the presence of significantly lower interfacial tensions behind the surfactant flood front. Interestingly, in Fig. 5A, we see that the TCE was actually falling under the force of gravity along the front formed between fresh water and the surfactant solution. As TCE fell through the bottom of the surfactant front, it encountered an environment not yet swept by the surfactant. Without the presence of surfactants, interfacial tensions remain high and the porous medium resisted invasion by nonwetting TCE. In this particular example, this did not halt the mobilized TCE, but rather redirected it to follow along a path where the TCE could remain mobile—namely downward and along the surfactant front. In this manner, the surfactant front forms a capillary barrier of sorts. Ahead of the surfactant front, interfacial tensions (and capillarity) remain high. Behind the surfactant front, low interfacial tensions markedly reduce capillary resistance to gravity-induced flow of TCE. Grubb and Sitar (1999) observed similar TCE migration along the co-solvent/fresh water interface. In their experiment, significant gravity override of the co-solvent front (rather than the presence of heterogeneities as in our case) resulted in a nonvertical interface. In Fig. 5A, we see that the TCE finger has passed through several layers of material. The finger originates from the pool formed from a layer of coarse sand and the finger has migrated through a layer of medium sand and a layer of medium-coarse sand, back into a layer of medium sand. In the reduced capillarity region behind the surfactant front, migration path appears to be only minimally influenced by textural heterogeneities. Similarly, Singletary et al. (1999) noted uniform downward flow of PCE through textural variations in low interfacial tension systems. In the photo in Fig. 5A, the tip of the TCE finger had just encountered a layer of fine sand and the TCE is beginning to pool above this layer. (This is the dark layer in the photo.) It is possible that even behind the surfactant front, this layer was able to offer some capillary resistance to flow due to its fine texture. However, it is likely that the surfactant front has progressed much more slowly through this layer due to its lower permeability. As can be seen in later figures, this layer provided only a temporary barrier to the mobilized TCE.

Migration from pool #5 can be seen in Fig. 4B,C. In contrast to the migration path from pool #2, the TCE moved straight downward due to the vertical nature of the surfactant front in this region. However, once the TCE finger encounters a change in texture (from medium-coarse sand to medium sand), it moved laterally and downward, again following the boundary of the surfactant front.

Fig. 5B shows migration from pool #7. (Look also at Fig. 4B,C.) Notice how TCE has moved against the hydraulic gradient and *upward* against gravity. The fact that the surfactant had not yet been able to penetrate the fine sand that forms the bottom of the aquifer prevented downward migration. In this pool, high interfacial tensions ahead of the front coupled with low interfacial tensions behind create a pressure differential that has driven TCE from the pool upstream into the invading fluid. Clearly, there is an additional mobilization mechanism active beyond simple gravity-instability under reduced capillarity. The specifics of these mechanics are discussed in detail in the section entitled, *Predicting the onset of mobilization*. Finally, we note that during the mobilization of pool #7, TCE was supplied from throughout the region where TCE was fully connected. This is

particularly well shown when we consider that pools #7 and #8 were connected via the large channel within the right manifold. The TCE feeding the upstream mobilization of pool #7 has come from throughout pool #7, but it has also come from pool #8, quite a distance away.

The photograph in Fig. 6A shows an intermediate stage of the displacement process (0.44 pore volumes of surfactant solution introduced). Widespread mobilization had occurred. Every pool of TCE that the surfactant front had reached was in the process of draining. Textural heterogeneities (that played so prominent a role in the initial emplacement of the TCE into a series of pools) had relatively little influence on this remobilization process. However, during this period, fine layers did exert some control on the mobilization structure allowing the formation of new TCE pools within the system that were subsequently mobilized when surfactant invaded the capillary barriers beneath these new pools. Downward mobilization typically began with formation of a TCE finger (as shown in Fig. 5A). However, as the rate of supply of TCE from the pool diminished over time, the fingers of TCE became much less continuous. Low interfacial tension between the two liquid phases behind the surfactant flood front allowed the TCE to easily break up into small blobs and droplets during downward migration. These blobs "rained down" through the formation with many blobs becoming trapped along the way.

The photograph and digital image shown in Fig. 6B,C show the configuration of the TCE once the surfactant front has traversed the sand-tank aquifer (2.6 pore volumes injected). By then, the mobilization phase had been completed and all TCE pools had drained. As can be seen from both the photograph and the digital image, the contents of the pools have been redistributed and eventually trapped as blobs at residual saturation. The photo shows that once behind the surfactant front, the TCE spilled vertically, moving downward until the mass was exhausted as a residual saturation. Residual blobs were left behind in all the facies the TCE passed through. Inspection of the digital image in Fig. 6C provides a summary and allows reconstruction of the mobilization process. For all the pools above the base of the aquifer, it is possible to track the migration path from each of the pools as they drained. The hydraulic gradient appears not to have influenced the migration path of the mobilized TCE.

Visual inspection of close-up photos and digital images (not shown) indicates that residual saturation may have been a function of facies texture. That is, finer grained facies appear to have had higher residual saturations than coarse-grained facies. However, residual saturations in all facies were reduced relative to the residual saturations observed prior to the introduction of the surfactant solution. Also, the residual blobs are trapped almost exclusively as singlets, blobs that reside only in a single pore. This contrasts with the observations of blob size and shape trapped under higher interfacial tension conditions where the vast majority of residual was found to be held as branched blobs extending over several to many pores (Conrad et al., 1992; Wilson et al., 1990; Mayer and Miller, 1992; Chatzis et al., 1983, 1998). We observed that these singlet blobs became trapped by two mechanisms. Some blobs became trapped through the snap-off mechanism (Wilson and Conrad, 1984; Chatzis et al., 1983) that occurred at the trailing edge of a TCE finger or at the trailing edge of a large migrating blob. Also, small spherical blobs raining down through the formation became trapped as they encountered smaller pore throats that impeded migration.

Here we note two positive (though relatively minor) aspects of this mobilization and retrapping as singlet blobs. (1) This redistribution has led to an increase in the surface area

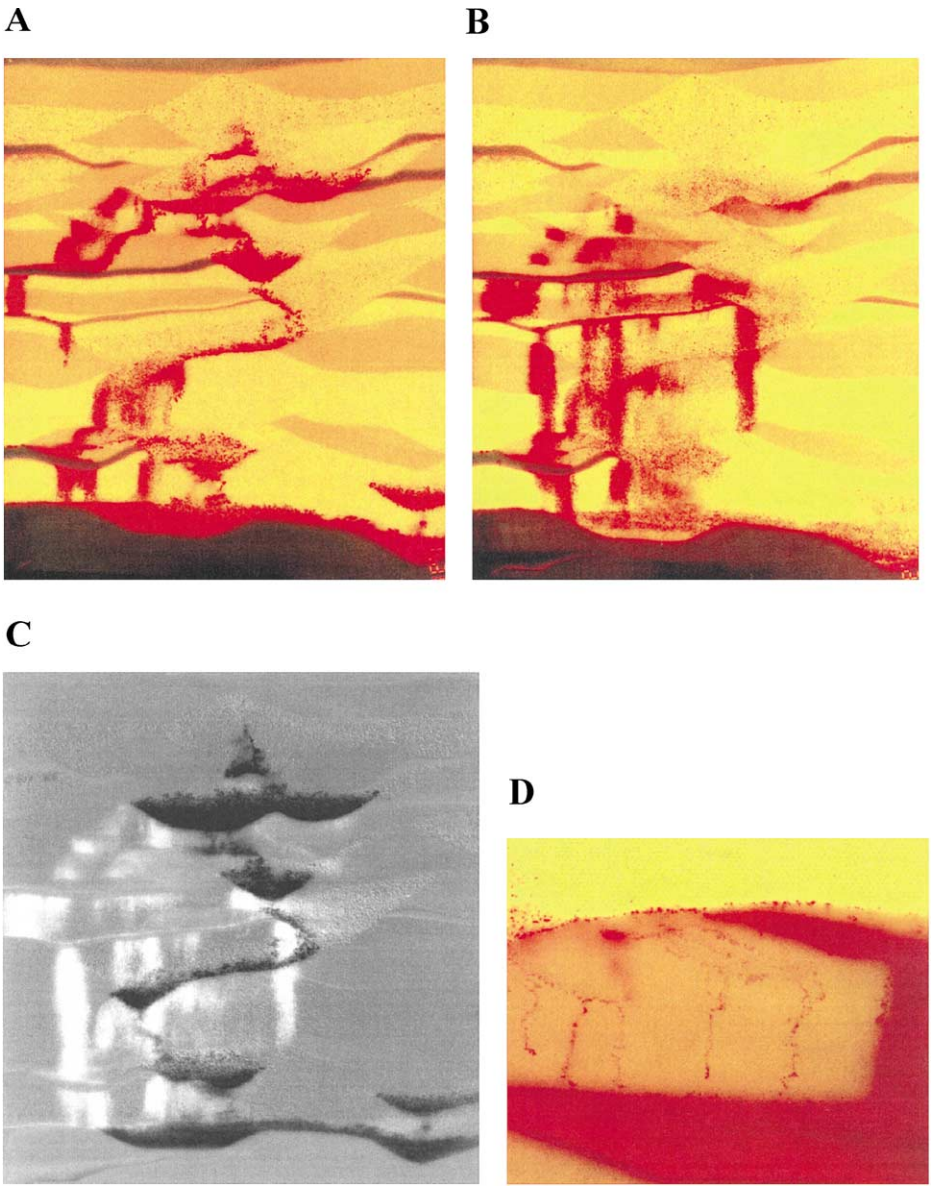

Fig. 6. Images tracking the progress of mobilization from the Aerosol MA surfactant experiment: (A) a photograph at 0.44 pore volumes; (B) a photograph showing the configuration of TCE within the aquifer once mobilization ceased (2.6 pore volumes); (C) an image showing differences in light intensity between a digital image taken at 2.6 pore volumes and an image taken prior to the start of the surfactant flood—dark regions show from where TCE has migrated, while white regions indicate regions where TCE has migrated into (gray indicates no change); (D) a close-up photograph from the lower left corner of the chamber showing that a significant amount of mobilized TCE penetrated into the fine sand aquitard.

to volume ratio for the TCE. In higher permeability regions where efficient delivery of the surfactant solution is possible, improved contact between the TCE and the surfactant should lead to improved solubilization. (2) Ironically, this redistribution as trapped residual blobs rather than primarily in pools, more closely approximates the preconception of DNAPL trapped primarily at a residual saturation. Thus, it more closely resembles the initial conditions imposed by many laboratory column experiments run to test proof-of-concept for surfactant-based remediations.

Unfortunately, the mobilization process has allowed TCE to penetrate into fine-grained facies that it was unable to penetrate prior to the introduction of surfactant solution. The close-up photo provided in Fig. 6D shows that TCE had penetrated into the fine sand aquitard that forms the base of the aquifer. Disconcertingly, a large proportion of the total TCE mass migrated down into this region.

Once all DNAPL has redistributed based on the lowered interfacial tensions, the rest of the experiment proceeds according to what we would expect for solubilization. Fig. 7A,B shows photographs taken at 3.2 and 7.3 pore volumes, respectively. TCE trapped in finer textured units was solubilized at a much lower rate. The digital images presented in Fig. 7C,D illustrate the progress of the solubilization process over time. Cool colors indicate the locations where solubilization occurred first. The progression from cool to warm colors tracks the evolution of the solubilization process. Notice that solubilization does not seem to advance uniformly from left to right. It appears that solubilization proceeds from outside to inside, with solubilization occurring first along the edges of the TCE-entrapment features and proceeding inward over time. This pattern of solubilization occurs presumably because the lower permeability to water in regions having trapped TCE creates an obstruction to flow causing water to preferentially travel around rather than through these features.

We concluded this experiment after introducing 7.3 pore volumes of Aerosol MA surfactant solution. At that time, a large majority of the residual TCE in the aquifer above the aquitard had been solubilized with some still remaining in fine-textured units. The significant mass mobilized into the aquitard also remained at the conclusion of the experiment. Since the surfactant flood largely bypassed this region, very little solubilization occurred. Finally, we note that it would also be unlikely that any characterization undertaken to track the progress of the remediation, such as a PIT test, would identify this mass as remaining in the subsurface. Consequently, this mass could potentially erroneously be considered to have been cleaned up, when in fact, the remediation problem has been made more intractable.

4.2. Tween 80 surfactant experiment

Our second surfactant flood was conducted using Tween 80, a nonionic ethoxylated sorbitan based surfactant. This surfactant has been used previously by several researchers (e.g., Singletary et al., 1999; Rathfelder et al., 1998; Walker et al., 1998). The surfactant composition was 5% by mass in de-aired, deionized water. Using a du Nouy ring tensiometer, we measured the interfacial tension between dyed TCE and the Tween 80 surfactant solution to be 9.0 dyn/cm. The measurement was taken after the surfactant solution had been in contact with the dyed TCE for 30 s, following ASTM procedure. We note, however, that Mason and Kueper (1996) measured interfacial tension as a function of

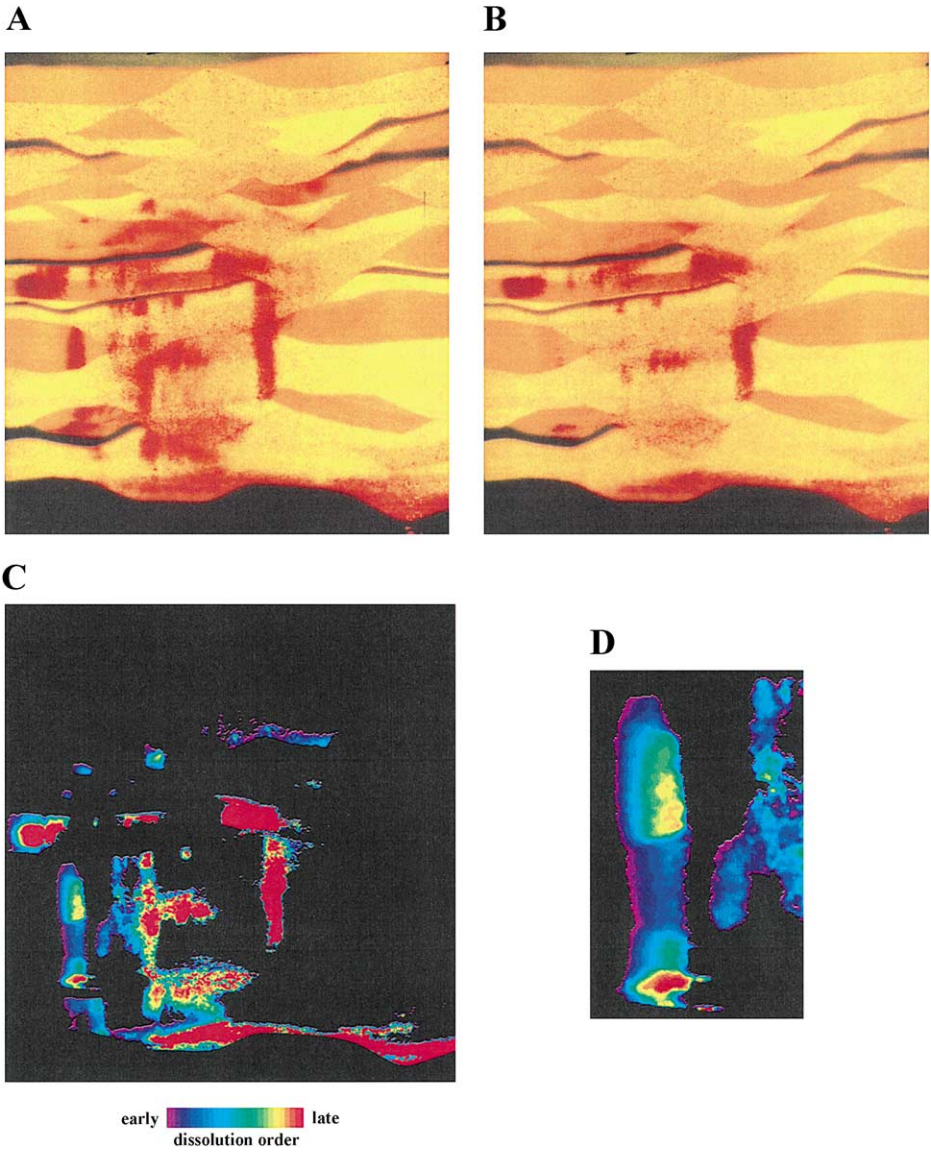

Fig. 7. Images showing solubilization of TCE in the Aerosol MA experiment: (A) a photograph of TCE remaining in the aquifer after 3.2 pore volumes of surfactant solution injected; (B) a photograph of TCE remaining at the conclusion of the experiment (after 7.3 pore volumes); (C) a composite image tracking the progress of TCE solubilization over time—cool colors indicate locations where TCE was solubilized away first, warmer colors indicate locations where TCE was solubilized away later, red regions still contained TCE at the conclusion of the experiment; (D) a close-up of the composite image from the lower left portion of the chamber showing the outside-to-inside pattern of solubilization with TCE contained in lower permeability regions dissolving away more slowly.

time and found that DNAPL/surfactant solution interfacial tension decreased slowly over time, dropping to less than one half its original value over the course of a week.

The dye pulse shown in Fig. 3 was injected prior to the beginning of the Tween 80 experiment and some dissolution of the TCE had already occurred. Fig. 3D shows the TCE as it was configured in the sand-filled chamber prior to invasion by the Tween 80 surfactant. Compare this photo with the one in Fig. 4A showing the TCE configuration prior to invasion by the Aerosol MA surfactant. Both the heterogeneity structure and the configuration of the TCE within the aquifer were very similar to that of the Aerosol MA surfactant experiment, with the TCE occupying the same sequence of pools. However, some differences are notable. There was a difference in injected TCE volume (67 ml TCE for the Aerosol MA experiment versus 54 ml TCE for the Tween 80 experiment). In addition, the TCE emplaced for the Tween 80 experiment experienced some dissolution during side-to-side aqueous flow of the blue dye pulse.

Fig. 8A shows a digital difference image that summarizes the mobilization process. This figure shows the difference in configuration of the TCE once the Tween 80 surfactant front has had opportunity to encounter all the pools (~ 0.7 pore volumes injected). Aside from the bottom pool (#7), all TCE pools have drained to a significant extent. However, unlike the Aerosol MA experiment, the pools have not drained completely. Above the somewhat depleted pools, a much larger residual saturation exists, demarcating the pool heights that existed prior to mobilization. As can be seen from the digital difference image, the mobilization of the TCE has been for the most part confined to migration via preexisting migration paths. For example, as pool #2 drained, it drained into pools #3, #4, and #5, and this drainage occurred along the path of the initial TCE invasion. Review of animations created from the digital images confirms this process for mobilization. However, because Tween 80 acts as a strong solubilizer, some of the loss of mass from each of the pools was due to solubilization.

Fig. 8B provides a digital image close-up of the region around pools #5 and #6. Notice that pool #5 has drained, leaving residual saturation above the smaller vestige of the pool that remains. Pool #6 below has drained entirely. The white region below pool #5 shows the only instance of drainage occurring outside the flow paths established during the initial TCE migration.

Pool #7 gained some additional mass due to drainage from the pools above. Yet, in contrast to the Aerosol MA experiment, the fine-sand aquitard retained its integrity and no TCE was mobilized into it directly from pool #7 due to reductions in interfacial tensions. Notice also that Fig. 8A shows some migration from the left edge of pool #7. Similar to the migration seen in the Aerosol MA experiment, the TCE has moved against the hydraulic gradient and *upward* against gravity. The white region in the extreme bottom right corner indicates that TCE has migrated beneath the aquitard. The source of this TCE is the outflow side manifold and drainage from pool #8. This is an artifact of a flaw in our TCE injection procedure that allowed redistribution to carry TCE into the manifold and does not indicate a problem with maintaining the integrity of the aquitard.

Let us contrast these results with the results from the Aerosol MA experiment. In the Aerosol MA experiment, capillarity became relatively unimportant and the TCE spilled vertically behind the surfactant front. In the Tween 80 experiment, the migration process illustrates that by maintaining higher interfacial tensions, capillarity continues to influence

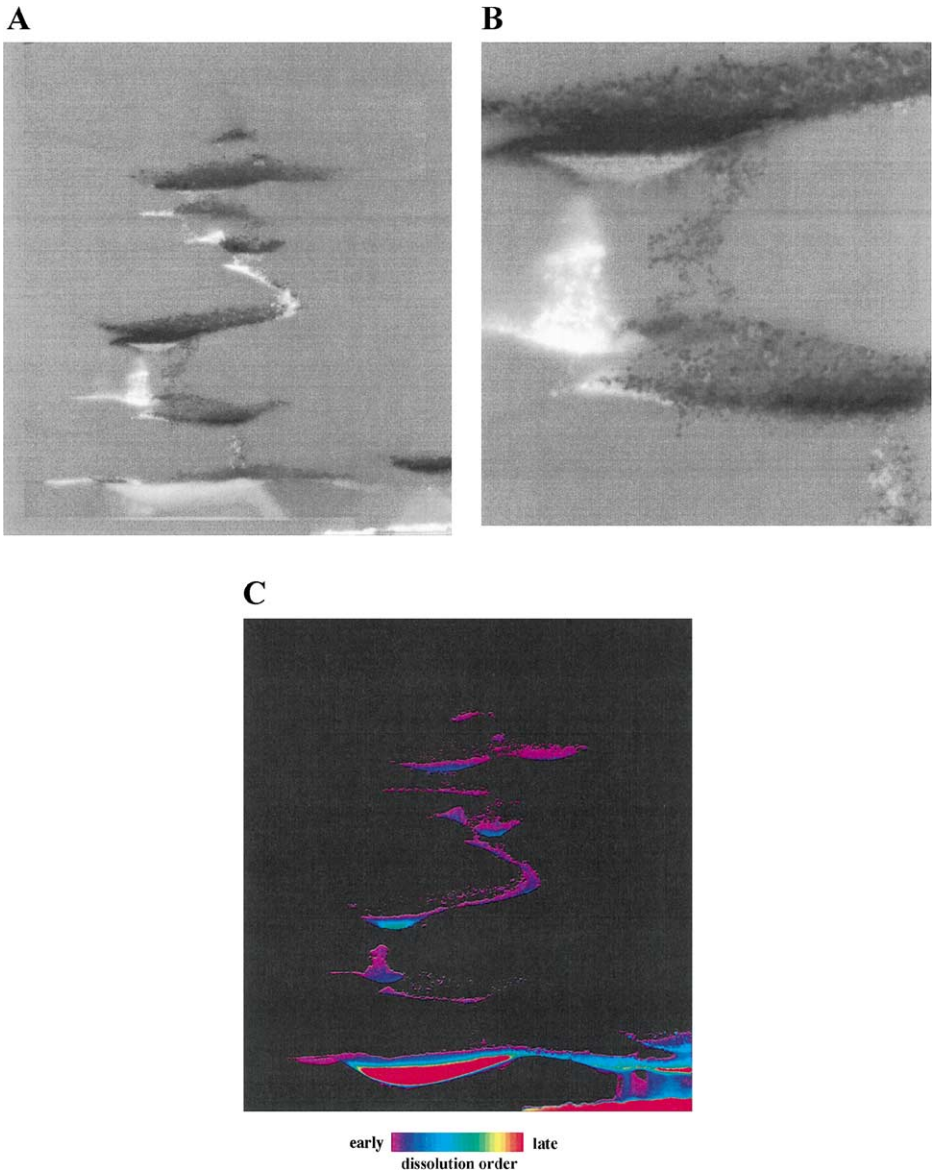

Fig. 8. Images from the Tween 80 surfactant experiment: (A) an image showing differences in light intensity between a digital image taken at once mobilization has ceased (~ 0.7 pore volumes) and an image taken prior to the start of the surfactant flood—white regions indicate regions where TCE has migrated into, while dark regions indicate regions where TCE has been removed either by mobilization or solubilization (gray indicates no change); (B) a digital difference image close-up showing pools #5 and #6; (C) a composite image tracking the progress of TCE solubilization over time—cool colors indicate locations where TCE was solubilized away first, warmer colors indicate locations where TCE was solubilized away later, the red region in pool #7 indicates the presence of TCE at the conclusion of the experiment.

migration behavior. Implications are that—although some portion of the TCE may still mobilize—maintaining higher interfacial tensions inhibits migration into fine-textured units.

The bulk-scale solubilization process is summarized in Fig. 8C. From inspection, it appears that solubilization occurred preferentially on the top of each pool. However, we believe this may have been an illusory artifact of redistribution of TCE within the pools as solubilization proceeded. We suspect that in these pools, solubilization proceeded from outside-to-inside, as the advecting surfactant solution came into contact with TCE along the periphery of the pools and mass was removed along all sides of the pools. However, as mass was removed from all sides, pressure equilibrium within the pool was maintained by preferentially vacating the pores along the top of the pools (where the gravity potential is lower). Pressure equilibrium influences on the dissolution of nonwetting phase blobs have been studied experimentally in fractures (Glass and Nicholl, 1995) and modeled using invasion percolation (Glass et al., 1998; Detwiler et al., 2001).

Solubilization from pool #7 proceeded more slowly. Especially after mobilization, this pool held a comparatively large mass of TCE. For large pools, the ratio of surface area to volume is smaller, and hence, mass transfer proceeded more slowly. Perhaps more importantly, the low permeability of the fine sand layer beneath the bottom of this pool markedly inhibited the aqueous-phase flow from reaching the bottom of the pool, effectively halving the surface area of organic phase exposed to rapidly moving surfactant solution. We observed the formation of a macroemulsion along the top of pool #7, indicating that was where contact between TCE and the surfactant solution was occurring. Observations of macroemulsion formation are not uncommon when working with non-ionic surfactants (e.g., Fountain et al., 1991; Pennell et al., 1994; Okuda et al., 1996; Oostrom et al., 1999).

This experiment was concluded after injection of 8.6 pore volumes of surfactant solution. As the experiment concluded, only a vestige of this pool remained. This is the red color at the bottom core of pool #7 as seen in Fig. 8C.

4.3. Potassium permanganate experiment

Yan and Schwartz (1999) have shown the basic mechanisms by which potassium permanganate oxidizes common chlorinated solvents. The reaction forms a number of intermediate constituents along the overall reaction pathway, but for TCE the endpoint reaction products are given as follows:

$$C_2Cl_3H + 2KMnO_4 \rightarrow 2MnO_2(s) + 2CO_2(g) + H^+ + 3Cl^- + 2K^+ \quad (1)$$

Fig. 9A shows the TCE as it was configured in the sand-filled chamber at the conclusion of the PIT test and just prior to invasion by the permanganate solution. Compare this photo with the one in Fig. 4A showing the configuration of the TCE prior to invasion by the Aerosol MA surfactant and Fig. 3D showing the configuration of the TCE prior to invasion by the Tween 80 surfactant. Once again, the configuration of the TCE within the aquifer was very similar to that of the previous experiments, with the TCE occupying the same sequence of pools as before. Again, some differences are notable. There was a difference in injected TCE volume (67 ml TCE for the Aerosol MA experiment versus 54 ml TCE for the Tween

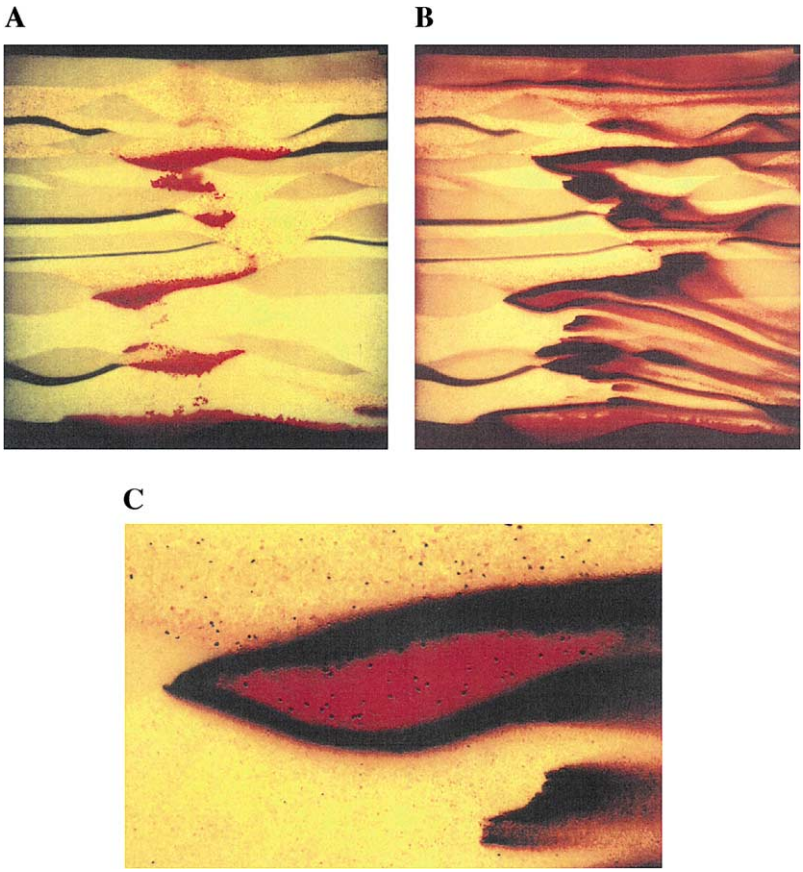

Fig. 9. Photographs from the potassium permanganate experiment: (A) a photograph showing the configuration of the TCE prior to the permanganate flood; (B) a photograph after the 1/3 pore volume slug of potassium permanganate solution had traversed the chamber (~1.2 pore volumes)—dark rinds around the pools are precipitated MnO_2; (C) a close-up photograph showing the MnO_2 rind surrounding pool #5.

80 experiment versus 37 ml for the permanganate experiment). In addition, the TCE emplaced for the permanganate experiment experienced dissolution during side-to-side aqueous flow of the PIT test.

We injected a pulse consisting of approximately 1/3 pore volume 1000-ppm potassium permanganate solution, followed by several pore volumes of water. We used relatively low concentrations for two purposes. First, injecting relatively low concentrations enhanced our ability to visually observe the interaction between permanganate solution and the TCE. Second, we wanted to avoid producing quantities of CO_2 in excess of the amount that would be readily dissolved into the aqueous phase. Schnarr et al. (1998) and Reitsma and Marshall (2000) observed significant gas production in their experiments. We used de-aired water to facilitate CO_2 dissolution. Our intent was to avoid CO_2 gas production that could increase pressure in the chamber, perhaps leading to bowing or cracking the glass.

The photograph in Fig. 9B shows the configuration of the TCE once the permanganate solution had traversed the flow field (~1.2 pore volumes injected). The permanganate solution had the opportunity to encounter all the pools. Interaction between the purple permanganate solution and the red-dyed TCE makes photographic interpretation of this experiment more difficult than the surfactant experiments. Upon contact of the permanganate solution with the TCE, MnO_2 has precipitated. Around the upstream, top, and bottom sides of each of the pools, a dark (brown to black) rind has formed. Suspended MnO_2 has also been carried downstream and been deposited along the way to create flow lines indicating the aqueous phase flow path. Fig. 9C provides a close-up of the rind that formed around pool #5. These qualitative visual results suggest that the MnO_2 rind has formed a low permeability barrier to flow. One exception to rind formation was pool #7, which formed a rind only at its upstream edge. Of course, low permeability of the fine sand bottom of the aquifer prevented permanganate solution from contacting the bottom of the pool while the upstream rind diverted flow away from the top of the pool. Similar to the surfactant experiments, the position of pool #7 at the bottom of the aquifer reduced contact between the TCE and the remedial solution.

Visual observation of color change indicated that a significant portion of the permanganate had reacted with TCE prior to reaching the far (right) edge of the flow field (with the exception of some permanganate that traversed the flow field at the extreme top and encountered no TCE). Perhaps needless to say, since the permanganate solution did not reduce interfacial tension, no mobilization of the TCE occurred.

A second 1/3 pore volume pulse of permanganate solution was injected. The flow pattern for the second pulse was noticeably different from the first pulse. Although the bulk flow rate was maintained at 5 ml/min, slower flow occurred in the mid-section of the chamber where the majority of large TCE pools resided, indicating lowered permeability in this region. As this pulse migrated, the magenta color persisted past the pools, indicating the presence of the MnO_2 rind has inhibited reaction between the permanganate and the TCE. Further downstream, some color dissipation was observed indicating that the permanganate solution was reacting with dissolved TCE emanating from the pools. However, the majority of the permanganate solution did reach the downstream reservoir without reacting. The experiment was discontinued after the second pulse of permanganate was pushed through the chamber due to clogging of the outflow manifold with MnO_2.

Since we had no immediate use for the chamber at the conclusion of this experiment, the experiment remained in its final condition, undisturbed for an extended period of time. Fig. 10 presents close-up photographs of pools #2, #3, and #4 taken 3 months after the conclusion of the experiment. Notice that pool #2 has drained and a new finger has emerged from the bottom of pool #4. We are not sure of the cause for the TCE movement and we are not sure whether it is related to the presence of the MnO_2 rinds. Tuck et al. (1997) demonstrated contact angle aging for multicomponent DNAPL/water interfaces. Contact angle aging changes wettability and reduces capillary resistance to displacement. The TCE movement could be related to contact angle aging or a reduction in interfacial tension over time thereby reducing capillary forces and it may or may not be related to chemical interaction with the MnO_2 rinds. However, it does indicate that the rinds probably cannot be relied on to provide isolation of the pools.

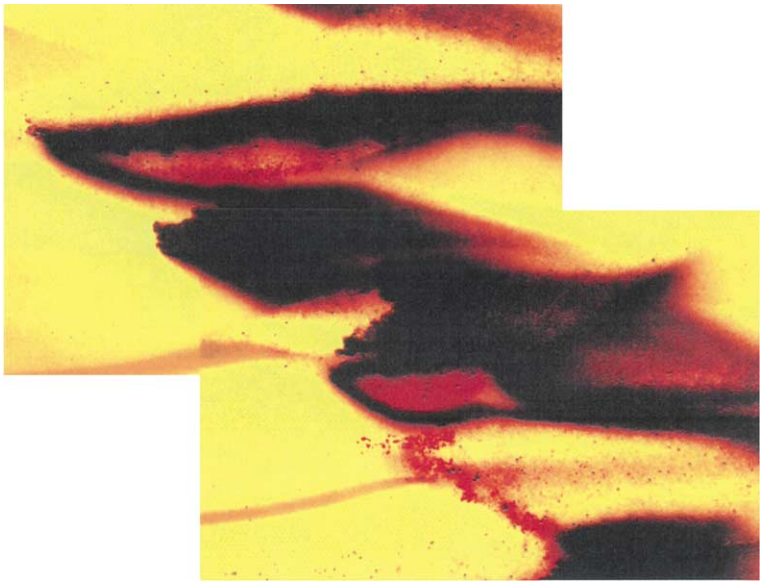

Fig. 10. A composite of two overlain close-up photographs showing the pools (#2, #3, and #4) 3 months after the conclusion of the permanganate experiment. Pool #2 has drained and a migrating finger of TCE has penetrated through the capillary barrier and the MnO_2 rind at the bottom of pool #4.

Upon drainage and disassembly of the chamber, we observed dark mineral coatings on the sand grains at the locations where the MnO_2 precipitation rinds had formed. Qualitatively, these mineral coatings appeared insufficient to cause the significant reductions in permeability observed to have occurred during the course of the experiment. To explore this issue further, we conducted a simple test tube experiment in which aqueous potassium permanganate solution was put in contact with TCE. Initially, the MnO_2 dispersed throughout the aqueous phase. However, with time (several hours to 1 day) the MnO_2 settled in the aqueous phase at the aqueous/organic interface. The MnO_2 observed in the test tube appeared to be much more substantive than the coatings on the sand grains we observed when we drained and disassembled the experimental chamber. The MnO_2 in the test tube appeared amorphous, perhaps even gel-like, and sufficiently substantive to impede contact between permanganate and TCE.

In the permanganate remediation experiment, some of the MnO_2 remained suspended and migrated downstream with the advecting aqueous phase, but the majority of the MnO_2 remained where it was formed at the aqueous/organic interface. Apparently, aqueous-phase advection did not provide sufficient viscous force to displace the majority of the MnO_2, and consequently, low-permeability rinds were able to form around the TCE pools. Perhaps the gel is resistant to shear. Perhaps a surface chemical reaction occurs that anchors the amorphous MnO_2 onto the sand grains. Whatever the mechanism, persistence of MnO_2 rinds impedes contact between permanganate solution and the TCE, limiting the rate of TCE oxidation, and thereby limiting the utility of the remediation technique. However, one

potentially fruitful avenue of experimentation to overcome this problem might be to investigate techniques for flocculating the MnO_2 rinds.

5. Predicting the onset of mobilization

We have observed mobilization in both surfactant floods. It is important that we better understand when mobilization will occur and the nature of the migration of the mobilized DNAPL. In the Aerosol MA surfactant experiment, we observed gravity-dominated mobilization where capillary forces exerted minimal influence on the migration pathway of the mobilized DNAPL. In contrast, in the Tween 80 surfactant experiment, we observed that a more modest reduction in interfacial tensions resulted in more modest mobilization. Importantly, we also observed that the preservation of some capillarity resulted in a migration pathway for the mobilized DNAPL that was constrained to coarse-textured units and generally restricted to the pathway of original DNAPL migration.

In this section, we develop analytical expressions to predict the onset of mobilization. We use these expressions to predict mobilization behavior for the Aerosol MA and Tween 80 surfactant experiments and compare these calculated results against experimental observations. Trapping and mobilization of residual nonwetting phase has been investigated by several researchers using the capillary number, N_C, the ratio of viscous to capillary forces, and the Bond number, N_B, the ratio of gravity to viscous forces.

$$N_C = \frac{q_w \mu_w}{\sigma} \tag{2}$$

$$N_B = \frac{\Delta\rho g R^2}{\sigma} \tag{3}$$

Here q_w is the specific discharge of water, μ_w is the viscosity of water, σ is the water/organic interfacial tension, $\Delta\rho$ is the density difference between the phases, g is the gravitational acceleration, and R is the representative grain size. Several studies using vertical displacements through packed columns (e.g., Morrow and Songkran, 1981; Zhou and Orr, 1995; Dawson and Roberts, 1997; Pennell et al., 1996) have shown the sum of viscous and gravity forces can be used to predict nonwetting phase saturation by quantifying when these forces begin to overcome the capillary forces that resist displacement of the nonwetting phase. However, Morrow and Songkran (1981) showed that for tilted columns, a modified Bond number ($N_B \sin\alpha$) underpredicted the displacement of the nonwetting phase relative to vertical displacements. Later, Pennell et al. (1996) derived an expression that combined the capillary and Bond numbers—called the trapping number—which demonstrated the importance of including gravity forces regardless of flow direction, even for horizontal flow where viscous and gravity forces operate normal to one another. They also studied the mobilization of trapped DNAPL using surfactants. In both vertical and horizontal displacements through packed columns, they observed downward migration of mobilized DNAPL droplets for high Bond number situations (that is, for the combination of coarse textured media and low interfacial tensions). They suggest employing the trapping number analysis when selecting surfactant formulations. The intent is to select surfactants having interfacial

tensions of sufficient magnitude to keep the trapping number below a critical value indicative of the onset of mobilization.

However, we note several departures between the assumptions contained within trapping number analysis and the situation seen in our surfactant experiments that may make implementation problematic for field-scale applications. First off, the trapping number considers the potential for mobilization of an organic phase present as trapped blobs at residual saturation, whereas we have seen from our experiments that the DNAPL resides predominantly in pools of continuous free phase DNAPL. The much smaller height of blobs relative to pool heights limit the length over which gravity forces operate.

Second, all the referenced experiments and theoretical developments consider 1-D displacements through homogeneous media. Of course, in heterogeneous media, Bond and capillary numbers change from one facies to another. Coarse-textured media have a larger ratio of gravity to capillary forces as controlled by R^2 in the numerator of the Bond number. The pools, whose potential for mobilization we wish to consider, exist in coarse-textured facies. However, any mobilization would commonly occur into fine-textured facies that form the capillary barrier to DNAPL migration. So it becomes unclear which unit—the coarse unit containing the pool or fine-textured unit that forms the capillary barrier—is more appropriate for calculating the Bond number. Likewise, we expect that calculating viscous forces may be problematic in a multidimensional flow system where the water phase is able to flow around pools. Although pools occur in coarse-textured units, at high DNAPL saturations, the relative permeability to water will be low and water flow can be expected to largely bypass the pools.

Finally, we note that these experiments and analyses assume that interfacial tensions remain spatially constant. This is reasonable for displacements without introduction of surfactants, or for cases where the organic phase exists as blobs since the advancing surfactant front will quickly envelop blobs that exist on the scale of several pores. However, this assumption poses problems for surfactant fronts encountering pools. This is the phenomenon observed in the Aerosol MA surfactant experiment and to a lesser extent in the Tween 80 experiment where markedly different interfacial tensions ahead and behind the surfactant front provides a mechanism that helps drive the mobilization process. We referred to this process above as the capillary bellows process. Similar to bellows, capillary forces push a bladder (formed by the interface between the organic phase in the pool and the surrounding water phase) to expel fluid out a hole in the bladder. Surfactant reaching the upstream edge of a pool locally decreases the interfacial tension creating a hole that allows for the release of capillary pressure. This capillary bellows mechanism (quantitatively discussed in more detail below) is not included in any analyses using Bond, capillary, or trapping numbers. While these dimensionless numbers provide insights in understanding the interplay between gravity, viscous, and capillary forces, their use in designing surfactant remedial systems is limited due to their tendency to underestimate the potential for mobilization.

We consider two simple analyses to predict the onset of mobilization from pools. In the first analysis, we set aside complications imposed by the capillary bellows process and consider the lowering of interfacial tensions everywhere around the pool. We refer to this as the standard drainage process. For this drainage process, we take the unit scale pool throbbing in our TCE injection experiment as our example. As was explained by Glass

et al. (2000), such pulsation occurs within a pool due to hysteresis in the capillary pressure for filling and vacating pores in the unit immediately underlying the pool. A pool continues to fill until sufficient pressure is built up to penetrate the underlying unit where upon the pool begins to drain. As the pool drains, DNAPL-filled pores in the pool and those just beneath the pool begin to depressurize. In the pores of the finger within the capillary barrier just beneath the pool, once the pressure decreases to the wetting entry value, they will be reinvaded with water and drainage of the pool will cease. Given easily obtainable parameter values for fluid and porous media properties, we have shown that maximum ($h_{\mathrm{p\ max}}$) and minimum ($h_{\mathrm{p\ min}}$) pool heights can be estimated with reasonable accuracy. For DNAPLs migrating under low flow rates where viscous forces within the DNAPL can be neglected, $h_{\mathrm{p\ max}}$ and $h_{\mathrm{p\ min}}$ as given by Glass et al. (2000) can be simplified to:

$$h_{\mathrm{p\,max}} = \frac{2\sigma}{\Delta\rho g}\left[\frac{1}{R_{\mathrm{nwb}}} - \frac{1}{R_{\mathrm{nwp}}}\right] \tag{4}$$

$$h_{\mathrm{p\,min}} = \frac{2\sigma}{\Delta\rho g}\left[\frac{1}{R_{\mathrm{wb}}} - \frac{1}{R_{\mathrm{wp}}}\right] \tag{5}$$

where the different R values represent the equivalent pore radii designated by subscripts for the nonwetting (nw) or wetting (w) fluids in the pool (p) or barrier (b) materials. Noting that in practice, the equivalent pore radii for wetting is roughly a factor of two larger than for nonwetting fluid invasion, we find that:

$$\frac{h_{\mathrm{p\,max}}}{h_{\mathrm{p\,min}}} \approx 2 \tag{6}$$

Returning to our mobilization problem, since the interfacial tension scales both $h_{\mathrm{p\ max}}$ and $h_{\mathrm{p\ min}}$, after the introduction of the surfactant we now have:

$$h_{\mathrm{p\,max\,s}} = \frac{\sigma_{\mathrm{s}}}{\sigma} h_{\mathrm{p\,max}} \tag{7}$$

$$h_{\mathrm{p\,min\,s}} = \frac{\sigma_{\mathrm{s}}}{\sigma} h_{\mathrm{p\,min}} \tag{8}$$

where the additional subscript denotes values in the presence of the surfactant. For simplicity, let us first consider the situation where all pools are at their lower value of $h_{\mathrm{p\ min}}$ before a remediation flood. From understanding of pool pulsation dynamics, a pool will not mobilize until $h_{\mathrm{p\ max\ s}}$ becomes lower than $h_{\mathrm{p\ min}}$. Thus, we see that as long as the reduction in surface tension is less than 1/2 the initial value, mobilization will not occur, regardless of the properties of the heterogeneous system. However, if the surfactant reduces the surface tension more than this amount, as was the case in our experiments, all pools will mobilize. Once again, considering the situation where all pools now drain to their lowest values of $h_{\mathrm{p\ min\ s}}$ (given by Eq. (8)) the amount of mobilization can be estimated.

As an example, let us consider the mobilization from pool #2 in the Tween 80 experiment. We examined the digital images to measure pool heights. Prior to mobilization and solubilization, we estimated the pool height to be between 1.7 and 2.4 cm. Let us take

this pool height as $h_{p\ min}$. Using values σ_s=9 dyn/cm and σ=27 dyn/cm (as reported in Glass et al., 2000), we calculate a final pool height in the presence of Tween 80 of between 0.6 and 0.8 cm. This value is in good agreement with the measured final pool height of 0.8 cm from image analysis. Of course, if σ_s is very low, such as in the Aerosol MA experiment, the pools will drain completely.

While the simple rule of thumb for mobilization (reduction of interfacial tension of 1/2 or greater) and the subsequent ability to calculate the mobilized volume is of great practical value within a heterogeneous system, we must recognize that our analysis is somewhat oversimplified. We know that initial pool heights ($h_{p\ initial}$) will not all be at $h_{p\ min}$ and likely range at all levels between $h_{p\ min}$ and $h_{p\ max}$. Thus, a reduction in surface tension such that:

$$h_{p\,initial} \geq \frac{\sigma_s}{\sigma} h_{p\,max} \tag{9}$$

will cause pool mobilization and the release of the drainable pool volume down to the final pool height ($h_{p\ min\ s}$, Eq. (8)) in the presence of the surfactant. So, the 1/2 rule of thumb will not be conservative. In fact, when considering a sequence of pools, the single pool analysis such as presented in Eq. (9) is still an oversimplification. We must recognize that when one pool mobilizes, it will release DNAPL that migrates to the next pool where, even if it would not have mobilized with interfacial tension lowering alone, it may exceed the $h_{p\ initial}$ for mobilization. Obviously, the evaluation of mobilization in the context of many pools of various sizes becomes more complicated by the presence of such cascade effects.

Moving to the capillary bellows process, we must recognize that when interfacial tension is not uniform everywhere—such as where markedly different interfacial tensions exist ahead and behind a surfactant front—then there is an additional driving force. Let us consider a simple case where a laterally advancing surfactant front encounters a pool. In this case, we are able to neglect gravity forces and simply compare the capillary pressures that exist on either side of the surfactant front as the surfactant front just reaches the pool. The pool will not begin to mobilize as long as:

$$\frac{\sigma_s}{\sigma} \geq \frac{R_{nwf}}{R_{wp}} \tag{10}$$

where R_{wp} is the effective radii for wetting phase invasion into the course unit that holds the pool of organic phase and R_{nwf} is the effective radii for nonwetting phase invasion into the finer textured unit just adjacent to the pool and just behind the surfactant front. Estimates for these effective radii are easily obtained from the wetting and drainage capillary pressure curves. Here we have used convenient notation denoting coarse and fine adjacent units because it is not uncommon for the pool boundary to occur along a textural interface between two adjacent facies. However, this need not always be the case. Consider, for example, the lateral mobilization from pool #7 shown in Fig. 5B where the left edge of the pool is dictated by topography rather than by an interface between facies. Here R_{nwf} becomes R_{nwp} and mobilization will occur when the interfacial reduction factor once again becomes smaller than 1/2.

Low organic/surfactant interfacial tensions and low textural contrast between the units encourages onset of the capillary bellows process. Once the condition for onset is met,

then the pool will continue to drain as long as the surfactant front maintains contact with the pool and as long as there is somewhere for the DNAPL to go behind the surfactant front. (As seen in Fig. 5A, gravity driven downward migration removes the DNAPL.) If the surfactant encounters the pool either from above (as in our photo of surfactant encountering the bottom pool, Fig. 5B) or below then gravity forces can easily be included in the force balance.

As before, let us use pool #2 as an example and examine capillary bellows induced mobilization for both the Aerosol MA and the Tween 80 experiments. Values of representative radii are the same for both experiments ($R_{wc} \sim 0.34$ mm for the coarse sand and $R_{nwf} \sim 0.09$ mm for the medium sand, as reported in Glass et al., 2000) as is the organic/water interfacial tension (σ=27 dyn/cm, as reported in Glass et al., 2000). Using a value of σ_s=0.62 dyn/cm for the Aerosol MA experiment, we see that the conditions of Eq. (7) are not met indicating that capillary bellows mobilization should result, in agreement with the experimental results. In contrast, for the Tween 80 experiment using a value of σ_s=9 dyn/cm, we see that the conditions of Eq. (7) are met indicating that capillary bellows mobilization should not result, again in agreement with the experimental results.

Taken together, Eqs. (6)–(10) provide the conditions for which surfactant solutions may induce mobilization from pools. Examination of these equations reveals that some basic knowledge of the geologic environment (that is, some idea of the textures of the units containing and surrounding the pools) is required to use these equations to estimate the propensity for mobilization—either by the standard drainage or the by capillary bellows process. Measurements of σ_s and σ are also required. Since mixed component or ''dirty'' DNAPLs are the reality at spill sites, estimates of σ obtained by measuring the interfacial tension between a reagent-grade solvent and water is not likely to be very representative. Jackson and Dwarakanath (1999) contend that spent degreasing solvents commonly have significantly lower interfacial tensions with groundwater than their pure counterparts due to the presence of large amounts of oil and grease and the incorporation of industrial detergents. Lowering the value of σ would reduce amount of DNAPL sequestered in pools as well as the potential for inducing its mobilization.

6. Conclusions

We conducted three bench-scale visualization experiments to remediate TCE from our heterogeneous analog aquifer. Two of these experiments involved using surfactants (Aerosol MA and Tween 80). In the third experiment, we injected a potassium permanganate solution to oxidize the TCE.

Because we have built realistic heterogeneous lithologic structures and we emplaced the TCE in the aquifer by allowing it to migrate as it would as if spilled, we get the TCE to reside in a similar configuration to what we might expect in an aquifer. Here, as in our previous work (Glass et al., 2000, 2001), the majority of the mass is held in high saturation pools. While the bottom of the aquifer provides an obvious location for a pool to form, pools can potentially form throughout the aquifer and at a variety of scales. Along the TCE migration path, pools become located in coarse facies overlying a unit having finer texture, which forms a capillary barrier to flow. This configuration, with the TCE primarily in pools,

provided the initial condition for each of our experiments. In each of these experiments, we have seen that the presence of pools has important implications for success of the remediation.

In each of the two surfactant experiments, we were attempting to recover TCE by solubilization. Addition of a surfactant greatly increases the rate of dissolution, but this comes at a cost. The interfacial tension between the organic phase and aqueous is always significantly reduced. Inadvertent downward mobilization of the DNAPL due to interfacial tension reduction (causing a reduction in the capillary forces holding the DNAPL in place) has long been a concern. Mobilization occurred in both the Aerosol MA and Tween 80 surfactant floods. In the Aerosol MA experiment, a more than 50-fold reduction in interfacial tension resulted in unrestrained mobilization. The most serious consequence was that the considerable reduction in interfacial tension reduced capillary forces to the point that TCE was able to penetrate into fine-textured units. As the TCE mobilized, it left behind a residual saturation along its migration path. Within the confines of the aquifer, some residual became trapped in fine-textured units. This slowed the solubilization process we had intended to facilitate, since surfactant supply to these units was hindered by low permeability. Even more deleterious, however, a significant quantity of TCE penetrated into aquitard at the base of the aquifer, making things far worse than before. With regard to TCE recovery, this surfactant flood was not considered a success.

In the Tween 80 experiment, reduction of interfacial tension was not as dramatic and the consequent mobilization, while not insignificant, was much more manageable. Since capillary forces maintained some effect, migration was constrained to preexisting pathways. TCE did not go into fine-textured regions, and more importantly, it did not penetrate the aquitard. The solubilization process was considered successful, with only a small pool of TCE remaining at the conclusion of the experiment.

From these experiments, we see that the propensity to mobilize during surfactant flooding was vastly enhanced by the fact that DNAPL was held in pools. Significant mobilization into fine-grained units (especially the aquitard) can make the problem worse. Remember the Hippocratic oath of remediation—first, do no harm. It is from these experiments that we discovered the ''capillary bellows'' process whereby markedly different interfacial tensions ahead and behind the surfactant front provides a mechanism for mobilization. As the surfactant front comes into contact with a pool, a strong capillary pressure gradient forms allowing contraction of the organic/aqueous interface, resulting in mobilization of the contents of the pool as the nonwetting phase is pushed toward the low interfacial tension region, through and behind the surfactant front. We developed analytical expressions to predict the onset of mobilization from pools considering both standard drainage and capillary bellows drainage.

In our third experiment, injection of a potassium permanganate solution resulted in precipitation of MnO_2, a reaction product, creating a low-permeability rind surrounding the DNAPL pools. Formation of this rind hindered contact between the permanganate and the DNAPL, limiting the effectiveness of the remediation. Again, explicit consideration of TCE configured predominantly into pools resulted in clogging that has not been seen in previous experiments where the DNAPL source zone existed as a residual saturation.

We believe that conducting sand tank bench scale experiments of remedial process provides a necessary step prior to pilot scale testing. Visualization of the remedial processes

was found to be an important component. Building sand tank lithologies evocative of aquifer lithologies was also found to be important. Experiments and analyses founded on an assumption of the nonwetting phase held predominantly as a residual saturation may have limited applicability to situations where mass is held predominantly in pools. Failure to consider the presence of DNAPLs held in pools during remediation design may lead to decreased performance or inadvertent downward mobilization. Experiments of this type are essential to developing improved understanding of fundamental physics and chemistry controlling remediation processes.

Acknowledgements

Each remediation experiment has benefited from direct collaboration with remedial technology experts. For the Aerosol MA surfactant flood, we worked with Alex Mayer and Lirong Zhong from Michigan Tech. For the Tween 80 surfactant flood, we worked with Kurt Pennell from Georgia Tech. For the permanganate oxidation, we worked with Jack Istok from Oregon State. Thanks to John Gilletly for help in constructing the experimental apparatus and to David Johnson for help in running the experiments. Thanks also to Bernie Kueper and Klaus Rathfelder for their helpful review comments. This research was supported by the Environmental Management Science Program, US Department of Energy under contract DE-AC04-94AL8500.

References

Abriola, L.M., Dekker, T.J., Pennell, K.D., 1993. Surfactant-enhanced solubilization of residual dodecane in soil columns: 2. Mathematical modeling. Environmental Science and Technology 27, 2341–2351.

Baran, J.R., Pope, G.A., Wade, W.H., Weerasooriya, V., Yapa, A., 1994. Microemulsion formation with chlorinated compounds of differing polarity. Environmental Science and Technology 28 (7), 1361–1366.

Boving, T.B., Brusseau, M.L., 2000. Solubilization and removal of residual trichloroethene from porous media: comparison of several solubilization agents. Journal of Contaminant Hydrology 42, 51–67.

Brewster, M.L., Annan, A.P., Greenhouse, J.P., Kueper, B.H., Olhoeft, G.R., Redman, R.D., Sander, K.A., 1995. Observed migration of a controlled DNAPL release by geophysical methods. Ground Water 33 (6), 977–987.

Brown, C.L., Delshad, M., Dwarakanath, V., Jackson, R.E., Londergan, J.T., Meinardus, H.W., McKinney, D.C., Oolman, T., Pope, G.A., Wade, W.H., 1999. Demonstration of surfactant flooding of an alluvial aquifer contaminated with dense nonaqueous phase liquid. In: Brusseau, M.L., Sabatini, D.A., Gierke, J.S., Annable, M.D. (Eds.), Innovative Subsurface Remediation: Field Testing of Physical, Chemical, and Characterization Technologies. ACS Symposium Series 725, pp. 64–85.

Chatzis, I., Morrow, N.R., Lim, H.T., 1983. Magnitude and detailed structure of residual oil saturation. SPE Journal 23 (2), 311–325.

Chatzis, I., Kuntamukkula, M.S., Morrow, N.R., 1998. Effect of capillary number on the microstructure of residual oil in strongly water-wet sandstones. SPE Reservoir Engineering 3 (3), 902–912.

Conrad, S.H., Wilson, J.L., Mason, W., Peplinski, W., 1989. Observing the transport and fate of petroleum hydrocarbons in soils and in groundwater using flow visualization techniques. In: Testa, S.M. (Ed.), Environmental Concerns in the Petroleum Industry. American Association of Petroleum Geologists, pp. 1–13.

Conrad, S.H., Mason, W.R., Peplinski, W.J., Wilson, J.L., 1992. Visualization of residual organic liquid trapped in aquifers. Water Resources Research 28 (2), 467–478.

Dawson, H.E., Roberts, P.V., 1997. Influence of viscous, gravitational, and capillary forces on DNAPL saturation. Ground Water 35 (2), 261–269.

Detwiler, R.L., Rajaram, H., Glass, R.J., 2001. Nonaqueous-phase-liquid dissolution in variable-aperture fractures: development of a depth-averaged computational model with comparison to a physical experiment. Water Resources Research 37 (12), 3115–3129.

Dwarakanath, V., Pope, G.A., 2000. Surfactant phase behavior with field degreasing solvents. Environmental Science and Technology 34, 4842–4848.

Dwarakanath, V., Kostarelos, K., Pope, G.A., Schotts, D., Wade, W.H., 1999. Anionic surfactant remediation of soil columns contaminated by nonaqueous phase liquids. Journal of Contaminant Hydrology 38, 465–488.

Fortin, J., Jury, W.A., Anderson, M.A., 1997. Enhanced removal of trapped non-aqueous phase liquids from saturated soil using surfactant solutions. Journal of Contaminant Hydrology 24, 247–267.

Fountain, J.C., Klimek, A., Beikirch, M.G., Middleton, T.M., 1991. The use of surfactants for in situ extraction of organic pollutants from a contaminated aquifer. Journal of Hazardous Materials 28, 295–311.

Fountain, J.C., Waddell-Sheets, C., Lagowski, A., Taylor, C., Frazier, D., Byrne, M., 1995. Enhanced removal of dense nonaqueous-phase liquids using surfactants. In: Sabatini, D.A., Knox, R.C., Harwell, J.H. (Eds.), Surfactant-Enhanced Subsurface Remediation. ACS Symposium Series 594, pp. 177–190.

Fountain, J.C., Starr, R.C., Middleton, T., Beikirch, M., Taylor, C., Hodge, D., 1996. A controlled field test of surfactant-enhanced aquifer remediation. Ground Water 34 (5), 910–916.

Glass, R.J., Nicholl, M.J., 1995. Quantitative visualization of entrapped phase dissolution within a horizontal flowing fracture. Geophysical Research Letters 22 (11), 1413–1416.

Glass, R.J., Nicholl, M.J., Yarrington, L., 1998. A modified invasion percolation model for low-capillary number immiscible displacements in horizontal rough-walled fractures: influence of local in-plane curvature. Water Resources Research 34 (12), 3215–3234.

Glass, R.J., Conrad, S.H., Peplinski, W., 2000. Gravity destabilized non-wetting phase invasion in macro-heterogeneous porous media: experimental observations of invasion dynamics and scale analysis. Water Resources Research 36 (11), 3121–3137.

Glass, R.J., Conrad, S.H., Yarrington, L., 2001. Gravity destabilized non-wetting phase invasion in macro-heterogeneous porous media: near pore scale macro modified invasion percolation simulation experiments. Water Resources Research 37 (5), 1197–1207.

Grubb, D.G., Sitar, N., 1999. Mobilization of Trichloroethene (TCE) during ethanol flooding in uniform and layered sand packs under confined conditions. Water Resources Research 35 (11), 3275–3289.

Hasegawa, M.H., Shiau, B.-J., Sabatini, D.A., Knox, R.C., Harwell, J.H., Lago, R., Yeh, L., 2000. Surfactant-enhanced subsurface remediation of DNAPLs at the former naval air station, Alemeda, California. In: Wickamanayake, G.B., Gavaskar, A.R., Chen, A.S.C. (Eds.), Treating Dense Nonaqueous-Phase Liquids (DNAPLs): Remediation of Chlorinated and Recalcitrant Compounds. Battelle Press, Ohio, pp. 219–226.

Holzmer, F.J., Pope, G.A., Yeh, L., 2000. Surfactant-enhanced aquifer remediation of PCE-DNAPL in low permeability sand. In: Wickamanayake, G.B., Gavaskar, A.R., Chen, A.S.C. (Eds.), Treating Dense Non-aqueous-Phase Liquids (DNAPLs): Remediation of Chlorinated and Recalcitrant Compounds. Battelle Press, Ohio, pp. 187–194.

Huang, K.-C., Chheda, P., Hoag, G.E., 2000. Pilot-scale study of in-situ chemical oxidation of trichloroethene with sodium permanganate. In: Wickamanayake, G.B., Gavaskar, A.R., Chen, A.S.C. (Eds.), Chemical Oxidation and Reactive Barriers: Remediation of Chlorinated and Recalcitrant Compounds. Battelle Press, Ohio, pp. 145–152.

Imhoff, P.T., Thyrum, G.P., Miller, C.T., 1996. Dissolution fingering during the solubilization of nonaqueous phase liquids in saturated porous media: 2. Experimental observations. Water Resources Research 32 (7), 1929–1942.

Jackson, R.E., Dwarakanath, V., 1999. Chlorinated degreasing solvents: physical–chemical properties affecting aquifer contamination and remediation. Ground Water Monitoring & Remediation 19 (4), 102–110.

Knox, R.C., Shau, B.J., Sabatini, D.A., Harwell, J.H., 1999. Field demonstration of surfactant-enhanced solubilization and mobilization at Hill Air Force Base, UT. In: Brusseau, M.L., Sabatini, D.A., Gierke, J.S., Annable, M.D. (Eds.), Innovative Subsurface Remediation: Field Testing of Physical, Chemical, and Characterization Technologies. ACS Symposium Series 725, pp. 49–63.

Kostarelos, K., Pope, G.A., Rouse, B.A., Shook, G.M., 1998. A new concept: the use of neutrally-buoyant microemulsions for DNAPL remediation. Journal of Contaminant Hydrology 34, 383–397.

Kueper, B.H., Redman, J.D., Starr, R.C., Reitsma, S., Mah, M., 1993. A field experiment to study the behavior of

tetrachloroethylene below the water table: spatial distribution of residual and pooled DNAPL. Ground Water 31 (5), 756–766.

Li, X.D., Schwartz, F.W., 2000. Efficiency problems related to permanganate oxidation schemes. In: Wickamanayake, G.B., Gavaskar, A.R., Chen, A.S.C. (Eds.), Chemical Oxidation and Reactive Barriers: Remediation of Chlorinated and Recalcitrant Compounds. Battelle Press, Ohio, pp. 41–48.

Longino, B.L., Kueper, B.H., 1995. The use of upward gradients to arrest downward DNAPL migration in the presence of solubilizing surfactants. Canadian Geotechnical Journal 32 (2), 296–308.

Martel, R., Gelinas, P.J., Desnoyers, J.E., Masson, A., 1993. Phase diagrams to optimize surfactant solutions for oil and DNAPL recovery in aquifers. Ground Water 31 (5), 789–800.

Martel, R., Gelinas, P.J., Desnoyers, J.E., 1998a. Aquifer washing by micellar solutions: 1. Optimization of alcohol–surfactant–solvent solutions. Journal of Contaminant Hydrology 29, 319–346.

Martel, R., Lefebvre, R., Gelinas, P.J., 1998b. Aquifer washing by micellar solutions: 2. DNAPL recovery mechanisms for an optimized alcohol–surfactant–solvent solution. Journal of Contaminant Hydrology 30, 1–31.

Mason, A.R., Kueper, B.H., 1996. Numerical simulation of surfactant enhanced solubilization of pooled DNAPL. Environmental Science and Technology 30 (11), 3205–3215.

Mayer, A.S., Miller, C.T., 1992. The influence of porous medium characteristics and measurement scale on pore-scale distributions of residual nonaqueous-phase liquids. Journal of Contaminant Hydrology 11, 189–213.

Mayer, A.S., Zhong, L., Pope, G.A., 1999. Measurement of mass-transfer rates for surfactant-enhanced solubilization of nonaqueous phase liquids. Environmental Science and Technology 33, 2965–2972.

Morrow, N.R., Songkran, B., 1981. Effect of trapping and buoyancy forces on non-wetting phase trapping in porous media. In: Shah, D.O. (Ed.), Surface Phenomena in Enhanced Oil Recovery. Plenum Press, New York, pp. 387–411.

Mott-Smith, E., Leonard, W.C., Lewis, R., Clayton, W.S., Ramirez, J., Brown, R., 2000. In situ oxidation of DNAPL using permanganate: IDC Cape Canaveral demonstration. In: Wickamanayake, G.B., Gavaskar, A.R., Chen, A.S.C. (Eds.), Chemical Oxidation and Reactive Barriers: Remediation of Chlorinated and Recalcitrant Compounds. Battelle Press, Ohio, pp. 125–134.

Nelson, M.D., Parker, B.L., Cherry, J.A., Al, T., 2000. Passive destruction of PCE DNAPL by potassium permanganate in a sandy aquifer. In: Wickamanayake, G.B., Gavaskar, A.R., Chen, A.S.C. (Eds.), Chemical Oxidation and Reactive Barriers: Remediation of Chlorinated and Recalcitrant Compounds. Battelle Press, Ohio, pp. 135–144.

Okuda, I., McBride, J.F., Gleyzer, S.N., Miller, C.T., 1996. Physiochemical transport processes affecting the removal of residual DNAPL by nonionic surfactant solutions. Environmental Science and Technology 30 (6), 1852–1860.

Oostrom, M., Hofstee, C., Walker, R.C., Dane, J.H., 1999. Movement and remediation of trichloroethylene in a saturated, heterogeneous porous medium: 2. Pump-and-treat and surfactant flushing. Journal of Contaminant Hydrology 37, 179–197.

Pennell, K.D., Jin, M., Abriola, L.M., Pope, G.A., 1994. Surfactant enhanced remediation of soil columns contaminated by residual tetrachloroethylene. Journal of Contaminant Hydrology 16, 35–53.

Pennell, K.D., Pope, G.A., Abriola, L.M., 1996. Influence of viscous and buoyancy forces on the mobilization of residual tetrachloroethylene during surfactant flushing. Environmental Science and Technology 30 (4), 1328–1335.

Pennell, K.D., Adinolfi, A.M., Abriola, L.M., Diallo, M.S., 1997. Solubilization of dodecane, tetrachloroethylene, and 1,2-dichlorobenzene in micellar solutions of ethoxylated nonionic surfactants. Environmental Science and Technology 31, 1382–1389.

Pope, G.A., Wade, W.H., 1995. Lessons from enhanced oil recovery research for surfactant-enhanced aquifer remediation. In: Sabatini, D.A., Knox, R.C., Harwell, J.H. (Eds.), Surfactant-Enhanced Subsurface Remediation. ACS Symposium Series 594, pp. 142–160.

Ramsberg, C.A., Pennell, K.D., 2000. Evaluation of surfactant formulations for treatment of a PCE-contaminated field site. In: Wickamanayake, G.B., Gavaskar, A.R., Chen, A.S.C. (Eds.), Treating Dense Nonaqueous-phase Liquids (DNAPLs): Remediation of Chlorinated and Recalcitrant Compounds. Battelle Press, Ohio, pp. 211–218.

Rathfelder, K.M., Taylor, T.P., Abriola, L.M., Pennell, K.D., 1998. Simulation of the surfactant-enhanced sol-

ubilization of PCE in bench-scale laboratory studies. In: Wickramanayake, G.B., Hinchee, R.E. (Eds.), Non-aqueous Phase Liquids: Remediation of Chlorinated and Recalcitrant Compounds. Battelle Press, Colombus, OH, pp. 91–96.

Reitsma, S., Marshall, M., 2000. Experimental study of oxidation of pooled NAPL. In: Wickamanayake, G.B., Gavaskar, A.R., Chen, A.S.C. (Eds.), Chemical Oxidation and Reactive Barriers: Remediation of Chlorinated and Recalcitrant Compounds. Battelle Press, Ohio, pp. 25–32.

Sabatini, D.A., Knox, R.C., Harwell, J.H., Wu, B., 2000. Integrated design of surfactant enhanced DNAPL remediation: efficient supersolubilization and gradient systems. Journal of Contaminant Hydrology 45, 99–121.

Schaerlaekens, J., Vanderborght, J., Merckx, R., Feyen, J., 2000. Surfactant enhanced solubilization of residual trichloroehtene: experimental and numerical analysis. Journal of Contaminant Hydrology 46, 1–16.

Schnarr, M., Truax, C., Farquhar, G., Hood, E., Gonullu, T., Stickney, B., 1998. Laboratory and controlled field experiments using potassium permanganate to remediate trichloroethylene and perchloroethylene DNAPLs in porous media. Journal of Contaminant Hydrology 29, 205–224.

Schroth, M.H., Ahearn, S.J., Selker, J.S., Istok, J.D., 1996. Characterization of Miller-similar silica sands for laboratory hydrologic studies. Soil Science Society of America Journal 60, 1331–1339.

Shiau, B.-J., Sabatini, D.A., Harwell, J.H., 1994. Solubilization and microemulsion of chlorinated solvents using direct food additive (edible) surfactants. Ground Water 32 (4), 561–569.

Singletary, M.A., Pennell, K.D., Ramsburg, A., 1999. Effects of soil layering and interfacial tension on DNAPL migration in subsurface environments. In: Schafran, C.G. (Ed.), Environmental Engineering 1999: Proceedings of the ASCE–CSCE National Conference on Environmental Engineering. American Society of Civil Engineers, Reston, VA, pp. 202–211.

St.-Pierre, C., Martel, R., Lefebvre, R., Hawari, J., 2000. Study of TCE (trichloroethene) recovery mechanisms through phase diagrams and sand column experiments. Proceedings, 1st Joint IAH-CNC and CGS Groundwater Specialty Conference, 53rd Canadian Geotechnical Conference. Canadian Geotechnical Society, pp. 173–180.

Taylor, T.P., Pennell, K.D., Abriola, L.M., Dane, J.H., 2001. Surfactant enhanced recovery of tetrachloroethylene from a porous medium containing low permeability lenses: 1. Experimental studies. Journal of Contaminant Hydrology 48, 325–350.

Tidwell, V.C., Glass, R.J., 1994. X-ray and visible light transmission for laboratory measurement of two dimensional saturation fields in thin slab systems. Water Resources Research 30 (11), 2873–2882.

Thompson, N.R., Hood, E.D., MacKinnon, L.K., 2000. Source zone mass removal using permanganate: expectations and potential limitations. In: Wickamanayake, G.B., Gavaskar, A.R., Chen, A.S.C. (Eds.), Chemical Oxidation and Reactive Barriers: Remediation of Chlorinated and Recalcitrant Compounds. Battelle Press, Ohio, pp. 9–16.

Tuck, D., Iversen, G.M., Pirkle, W.A., Rulison, C., Denham, M.E., 1997. Capillary barriers and time-dependent wetting relationships: effects of complex DNAPL components. EOS Transactions, American Geophysical Union 78 (4), F289, abstract in.

Urynowicz, M.A., Siegrist, R.L., 2000. Chemical degradation of TCE DNAPL by permanganate. In: Wickamanayake, G.B., Gavaskar, A.R., Chen, A.S.C. (Eds.), Chemical Oxidation and Reactive Barriers: Remediation of Chlorinated and Recalcitrant Compounds. Battelle Press, Ohio, pp. 75–82.

Walker, R.C., Hofstee, C., Dane, J.H., Hill, W.E., 1998. Surfactant-enhanced removal of PCE in a nominally two-dimensional, saturated, stratified porous medium. Journal of Contaminant Hydrology 34, 17–30.

Wilson, J.L., Conrad, S.H., 1984. Is physical displacement of residual hydrocarbons a realistic possibility in aquifer restoration? Proceedings, Petroleum Hydrocarbons and Organic Chemicals in Ground Water: Prevention, Detection, and Restoration. National Water Well Association, Dublin, OH, pp. 274–298.

Wilson, J.L., Conrad, S.H., Mason, W.R., Peplinski, W., Hagan, E., 1990. Laboratory investigation of residual liquid organics from spills, leaks, and the disposal of hazardous wastes in groundwater. EPA/600/6-90/004.

Yan, Y.E., Schwartz, F.W., 1999. Oxidative degradation and kinetics of chlorinated ethylenes by potassium permanganate. Journal of Contaminant Hydrology 37, 343–365.

Zhong, L., Mayer, A., Glass, R.J., 2001. Visualization of surfactant-enhanced nonaqueous phase liquid mobilization and solubilization in a two-dimensional micromodel. Water Resources Research 37 (3), 523–537.

Zhou, D., Orr, F.M., 1995. The effects of gravity and viscous forces on residual nonwetting-phase saturation. In Situ 19 (3), 249–273.